



HAL
open science

Soil chemistry, elemental profiles and elemental distribution 1 in nickel hyperaccumulator species from New Caledonia

Vidiro Gei, G. Echevarria, P.D. Erskine, Sandrine Isnard, Bruno Fogliani, E. Montargès-Pelletier, Tanguy Jaffré, K.M. Spiers, J. Garrevoet, Antony van Der Ent

► To cite this version:

Vidiro Gei, G. Echevarria, P.D. Erskine, Sandrine Isnard, Bruno Fogliani, et al.. Soil chemistry, elemental profiles and elemental distribution 1 in nickel hyperaccumulator species from New Caledonia. *Plant and Soil*, 2020, 457, pp.293-320. 10.1007/s11104-020-04714-x . hal-02972020

HAL Id: hal-02972020

<https://hal.science/hal-02972020v1>

Submitted on 19 Nov 2020

HAL is a multi-disciplinary open access archive for the deposit and dissemination of scientific research documents, whether they are published or not. The documents may come from teaching and research institutions in France or abroad, or from public or private research centers.

L'archive ouverte pluridisciplinaire **HAL**, est destinée au dépôt et à la diffusion de documents scientifiques de niveau recherche, publiés ou non, émanant des établissements d'enseignement et de recherche français ou étrangers, des laboratoires publics ou privés.

1 **Soil chemistry, elemental profiles and elemental distribution**
2 **in nickel hyperaccumulator species from New Caledonia**

3
4 Vidiro Gei¹, Guillaume Echevarria^{1,2}, Peter D. Erskine¹, Sandrine Isnard^{3,4}, Bruno Fogliani⁵,
5 Emmanuelle Montargès-Pelletier⁶, Tanguy Jaffré^{3,4}, Kathryn Spiers⁷,
6 Jan Garrevoet⁷, Antony van der Ent^{1,2*}

7
8 ¹Centre for Mined Land Rehabilitation, Sustainable Minerals Institute,
9 The University of Queensland, Australia.

10
11 ²Université de Lorraine – INRAE, Laboratoire Sols et Environnement, UMR 1120, France.

12
13 ³AMAP, Université de Montpellier, IRD, CIRAD, CNRS, INRAE, Montpellier, France.

14
15 ⁴AMAP, IRD, Herbier de Nouméa, Nouméa, New Caledonia.

16
17 ⁵Institut Agronomique néo-Calédonien (IAC), Equipe ARBOREAL (AgricultuRe
18 BiOdiveRsité Et vAlorisation), New Caledonia.

19
20 ⁶Laboratoire Interdisciplinaire des Environnements Continentaux, CNRS,
21 Université de Lorraine, France.

22
23 ⁷Photon Science, Deutsches Elektronen-Synchrotron DESY, Germany.

24
25 * Corresponding author: a.vanderent@uq.edu.au

26 Phone: +61 (07) 3346 4003

27

28 **ABSTRACT**

29 **Aims** This study aimed to establish elemental profiles and to spatially resolve the elemental
30 distribution in five New Caledonian woody Ni hyperaccumulator plant species (*Geissois*
31 *pruinosa* var. *pruinosa*, *Homalium francii*, *Hybanthus austrocaledonicus*, *Psychotria*
32 *gabriellae*, and *Pycnandra acuminata*) originating from the Cunoniaceae, Salicaceae,
33 Violaceae, Rubiaceae, and Sapotaceae families respectively.

34 **Methods** Using synchrotron-based micro-X-ray Fluorescence (μ XRF) imaging of different
35 plant tissues, from the roots to the shoots and reproductive organs, this study aimed to clarify
36 how distribution patterns of nickel, and other physiologically relevant elements, differ
37 between these species.

38 **Results** The results show that the tissue-level and cellular-level distribution of nickel in *P.*
39 *gabriellae*, *H. austrocaledonicus*, *G. pruinosa* var. *pruinosa*, and *H. francii* conform with the
40 majority of studied Ni hyperaccumulator plant species globally, including (temperate)
41 herbaceous species, with localization mainly in epidermal cells and phloem bundles.
42 However, *P. acuminata* has nickel-rich laticifers, which constitute an independent network of
43 cells that is parallel to the vascular bundles and are the main sink for nickel.

44 **Conclusions** Synchrotron-based micro-X-ray Fluorescence (μ XRF) is a powerful method for
45 investigating how metal hyperaccumulation influences acquisition and spatial distribution of
46 a wide range of elements. This non-invasive method enables to investigate the *in vivo*
47 distribution of multiple elements and the structure and organisation of cells (*e.g.* laticifers).

48

49 **Key words:** *Hyperaccumulator; Elemental distribution; Latex; X-ray Fluorescence*
50 *Microscopy.*

51

52 1. INTRODUCTION

53 Hyperaccumulators are unusual plants that accumulate particular metals or metalloids in their
54 living tissues to levels that are 2–3 orders of magnitude greater than is normal for most plants
55 growing on similar soils (van der Ent et al. 2012; Reeves et al. 2018a,b). Nickel
56 hyperaccumulator plants are defined as plants with Ni concentrations in leaves $>1000 \mu\text{g g}^{-1}$
57 dry weight (Jaffré et al. 1976; Reeves 2003; van der Ent et al. 2013). Discovering
58 hyperaccumulators and understanding their ecology could lead to identifying potential
59 species to be utilized in novel phytotechnologies such as agromining for phytoextraction of
60 valuable metals. They could be used in accumulating trace metals in naturally-mineralised
61 agricultural soils, low grade ores, mine tailings, or mineral processing wastes (Chaney 1983;
62 van der Ent et al. 2015a); and then harvested and processed to extract high-grade bio-ore or
63 ‘eco-catalysts’ (Brooks et al. 1998; Brooks and Robinson 1998; Chaney et al. 2007; Losfeld
64 et al. 2015b). Nickel phytomining is envisaged to become transformative in the rehabilitation
65 of tropical laterite mining operations as part of rehabilitation strategies (van der Ent et al.
66 2013; 2015a; Losfeld et al. 2015a,b; Erskine et al. 2018).

67

68 Currently, there are approximately 500 documented Ni hyperaccumulators worldwide
69 (Reeves et al. 2018a). The majority of the Ni hyperaccumulators have been recorded in Brazil
70 (130) (Reeves et al. 2007), Southern Europe and Minor Asia (80–90) (Brooks et al. 1979;
71 Adıgüzel and Reeves 2012), New Caledonia (65) (Jaffré et al. 2013; van der Ent et al.
72 2015c), and Malaysia (24) (van der Ent et al. 2015a,b; 2018c). Recent screening of herbarium
73 samples using a portable XRF instrument in New Caledonia has revealed the existence of 99
74 Ni hyperaccumulators and 74 Mn hyperaccumulators (11 known previously), meaning that
75 more hyperaccumulators are to be discovered with such fast and non-destructive methods
76 (Gei et al. 2018; 2020). One of the most unusual Ni hyperaccumulators is the tree *Pycnanandra*
77 (formerly *Sebertia*) *acuminata*, endemic to New Caledonia, whose latex contains up to 257
78 mg Ni g^{-1} dry latex (Jaffré et al. 1976; Jaffré et al. 2018). Hyperaccumulation is an extreme
79 phenotypic expression of transition element metabolic regulation in plants, which involves
80 specific transporters and sequestration of metal ions and chelates in specific sink tissues
81 (Krämer et al. 2007; Andresen et al. 2018). Hence, knowledge of the specific sequestering
82 and transport mechanisms within these hyperaccumulating plants is crucial to better
83 understand this phenomenon (van der Ent et al. 2017a,b). The frequent occurrence of
84 hyperaccumulation in a number of different clades suggests that Ni hyperaccumulation

85 evolved repeatedly in different lineages (Pollard et al. 2002; Krämer 2010), but it is unknown
86 whether physiological mechanisms of hyperaccumulation differ between the phylogenetic
87 groups (*i.e.* whether non-related hyperaccumulating species have similar eco-physiological
88 processes – inferred from cellular and tissue-level elemental distribution – associated with
89 hyperaccumulation).

90

91 Our understanding of the diversity of Ni hyperaccumulation mechanisms is limited because
92 studies on the spatial elemental distribution in tissues and cells have only been performed for
93 less than 10% of the >500 Ni hyperaccumulating plant species known globally (Mesjasz-
94 Przybyłowicz et al., 2016). Most of the studies initially conducted concerned small,
95 herbaceous plants from the families Brassicaceae, Asteraceae, and Celastraceae (*e.g.* *Alyssum*
96 (now *Odontarrhena*), *Noccaea* (formerly *Thlaspi*), *Berkheya*, *Senecio*, and *Stackhousia*) and
97 the leaves were typically the main analysed parts, while stems and roots were less often
98 investigated (Mesjasz-Przybyłowicz and Balkwill 1994; Mesjasz-Przybyłowicz et al.
99 1996a,b, 1997a,b,c, 2001a,b, 2007; Küpper et al., 2001; Bhatia et al. 2003, 2004; Broadhurst
100 et al. 2004, 2009; McNear et al. 2005; Tappero et al. 2007). The only tropical woody shrub
101 analysed was *Hybanthus floribundus* (Violaceae) for which Ni was mainly reported in the
102 leaf epidermis (Bidwell et al., 2004 Kachenko et al. 2008). There was also a short report on
103 species from the genera *Phyllanthus* (Phyllanthaceae), *Euphorbia* and *Leucocroton*
104 (Euphorbiaceae) from Cuba which reported that Ni concentration was highest in laticifers of
105 all the species, which all had latex (Berazaín et al. 2007), but it confirmed that leaf epidermis
106 was the storage location for all species studied. For the majority of investigated Ni
107 hyperaccumulator plant species, Ni is *a priori* preferentially accumulated in foliar epidermal
108 cells (Mesjasz-Przybyłowicz and Balkwill 1994 ; Mesjasz-Przybyłowicz et al. 1996a,b,
109 1997b,c, 2001b; Küpper et al. 2001; Bidwell et al. 2004; Bhatia et al. 2004; Broadhurst et al.
110 2004) with the exception of *Berkheya coddii*, where it occurs at high concentrations in the
111 palisade parenchyma (Groeber et al. 2015). The accumulation of Ni in leaf vacuoles as
112 complexes with organic acids is often interpreted as a mechanism of metal detoxification and
113 maintaining homeostasis (Seregin 2006). Recently, several detailed studies on tropical woody
114 shrubs and trees of the genera *Phyllanthus*, *Glochidion* (Phyllanthaceae), and *Rinorea*
115 (Violaceae) shed more light on cellular and sub-cellular distribution by using X-ray
116 Fluorescence Microscopy (μ XRF) and Proton Induced X-ray Emission (PIXE) techniques,
117 which provided highly resolved mapping and low limits of detection (van der Ent et al.

118 2017a,b, 2018b). These studies have shown that in phylogenetically distant species there is
119 remarkably similar chemical form and distribution of Ni within plant organs and tissues.
120 This study is a comparative assessment of elemental concentrations and distribution in
121 distantly related species from New Caledonia to establish whether similar patterns of Ni
122 hyperaccumulation mechanisms, observed so far globally, hold true for woody New
123 Caledonian hyperaccumulator plants. Therefore, synchrotron μ XRF was used to produce
124 highly resolved elemental mapping across different tissues in an array of species that occur in
125 New Caledonia. The model plants analysed in this study were chosen to be as representative
126 as possible of New Caledonian hyperaccumulator lineages (Fig. 1). The five selected species
127 represent five families and four plant orders (Ericales, Gentianales, Malpighiales, Oxalidales)
128 known to contain hyperaccumulator species worldwide. We aimed to investigate whether
129 distribution patterns of Ni at the cellular and tissue level in the roots, stem, and leaves, and
130 those of other physiologically relevant elements (*e.g.* Ca, K, Mn, Co, Zn), differ among these
131 species.

132

133 **2. MATERIALS AND METHODS**

134

135 **2.1 Species ecology** – All five taxa (*Geissois pruinosa* var. *pruinosa*, *Homalium francii*,
136 *Hybanthus austrocaledonicus*, *Psychotria gabriellae*, and *Pycnandra acuminata*) (Fig. 1) are
137 endemic to New Caledonia and grow on soils derived from ultramafic bedrock and outcrops.
138 All taxa have a wide distribution in New Caledonia (Fig. 2). *Homalium francii*, *H.*
139 *austrocaledonicus*, *P. gabriellae*, and *P. acuminata* occur in dense humid forest, the first
140 three species being common understory shrubs, whereas the latter is an uncommon upper
141 mid-story to canopy tree (Swenson and Munzinger 2010). *Geissois pruinosa* is an
142 ecologically ubiquitous species that occurs in maquis, most often in forest edges and
143 sometimes in dense humid forests, however the var. *pruinosa* is restricted to the southern part
144 of New Caledonia (Jaffré et al. 1979; Hopkins et al. 2014). These taxa are ultramafic
145 obligates, except for *Homalium francii* (Jaffré and Veillon 1990) and *Hybanthus*
146 *austrocaledonicus* (Paul et al. 2020) which also occur on other types of soils.

147

148 **2.2 Collection of plant samples and preparation** – All species were collected in New
149 Caledonia (Fig. 2). All samples were collected from natural populations in the Parc
150 Provincial de la Rivière Bleue, except for *Geissois pruinosa* var. *pruinosa* which was
151 collected at Monts des Koghis. Branch segments were collected from shrubs or obtained

152 from the canopy of mature trees with a pole pruner, packed in moist paper and kept in sealed
153 plastic bags, then brought to the PETRA III Synchrotron at DESY (Deutsches Elektronen-
154 Synchrotron, Hamburg, Germany) in a fresh state. In addition, tissue samples were excised
155 with a razor blade in the field and immediately shock-frozen using a metal mirror technique
156 in which the samples were pressed between a block of copper (Cu)-metal cooled by liquid N₂
157 and a second cooled Cu-metal block attached to a Teflon holder. This ensured extremely fast
158 freezing of the plant tissue samples to prevent cellular damage by ice crystal formation. The
159 frozen samples were then wrapped in aluminium (Al) foil, transported and subsequently
160 stored in a cryogenic container (at least -190°C) until further processing (*e.g.* sectioning and
161 mounting for μ XRF analysis as described below).

162
163 Freeze-dried specimens were prepared by sealing frozen samples in Ultralene film held onto
164 XRF sample cups (polypropylene, 6 μ m) with small holes punctured in the film for sublimed
165 water to escape. The freeze-drying process started at -196°C by inserting the framed frozen
166 samples onto a large steel block cooled in liquid nitrogen. The cooled block with samples
167 was then loaded into the freeze-drying machine and vacuum-pumped and set to -85°C.
168 Freeze-drying then progressed very slowly (by changing the set temperature with 5°C
169 increments) over the course of four days until room temperature was reached.

170
171 **2.3 Light microscopy and histochemistry** – Plant tissue samples were fixed in 3%
172 glutaraldehyde upon collection. Sections of 50–100 μ m thickness were obtained with a
173 vibratome (Leica VTS1000) after embedding in agarose and stained with 1% toluidine blue
174 to reveal anatomical features to assist in the interpretation of the element maps (Supporting
175 Information Figure S1 and S2).

176
177 **2.4 Soil sampling and determination of chemical properties** – Soil samples were taken
178 from near the base of each plant from which the tissue samples were also collected in the
179 Parc Provincial de la Rivière Bleue (Table 1). In total three soil samples were collected for *G.*
180 *pruinosa* var. *pruinosa*, three for *P. gabriellae* and one for *H. austrocaledonicus* and one for
181 *Pycnandra acuminata*. *Homalium francii* was collected very close to the *P. acuminata* so the
182 habitat elemental concentration values would be similar, hence no sample was collected. The
183 soil samples were taken with a plastic scoop from a depth of 10–20 cm. These soil samples
184 were air-dried and sieved (<2 mm). Sub-samples (~300 mg) were digested using 9 mL 70%

185 HNO₃ and 3 mL 37% HCl per sample in a microwave digester (Milestone Start D) for 1.5 h
186 and diluted to 40 mL with ultrapure water before analysis to obtain pseudo-total elemental
187 concentrations. Soil pH was measured in a 1:2.5 soil:water mixture after 2 h of shaking.
188 Exchangeable trace elements were extracted in 0.1 M Sr(NO₃)₂ at a soil:solution ratio of 1:4
189 (10 g soil with 40 ml solution) and 2 h shaking time (adapted from Kukier and Chaney 2001).
190 As a means of estimating potentially phytoavailable trace elements, diethylenetriamine penta-
191 acetic acid (DTPA-extractant) was used according to the method of Becquer et al. (1995)
192 which was adapted from the original method by Lindsay and Norvell (1978), with the
193 following modifications: exclusion of triethanolamine (TEA), pH adjusted to 5.3, 5 g soil
194 used with 25 mL extractant to prevent saturation of the DTPA, and an extraction time of 1 h.

195

196 **2.5 Chemical analysis of bulk tissue samples and soil extracts** – Plant tissue samples
197 (leaves, bark, branches, roots, fruits, flowers) for bulk chemical analysis were collected in
198 the field from the same plants. Latex was collected by cutting the bark of *P. acuminata*.
199 These samples were dried at 70°C for five days in a drying oven. The dried plant tissue
200 samples were subsequently ground and digested using 4 ml HNO₃ (70%) in a microwave
201 oven (Milestone Start D) for a 45-minute programme and diluted to 30 mL with ultrapure
202 water (Millipore 18.2 MΩ·cm at 25°C) before analysis with ICP-AES (Varian Vista Pro II)
203 for Ni, Co, Cr, Cu, Zn, Mn, Fe, Mg, Ca, Na, K, S, and P. Soil extracts were also analysed
204 using ICP-AES for the same elements. In-line internal addition standardization using yttrium
205 was used to compensate for matrix-based interferences.

206

207 **2.6 X-ray fluorescence microscopy (μXRF)** – The X-ray fluorescence microscopy
208 experiment was undertaken at Beamline P06 at the PETRA III (Deutsches Elektronen-
209 Synchrotron; DESY, Hamburg, Germany), a 6 GeV 3rd Generation Synchrotron Radiation
210 Source. The undulator beam was monochromatised with a cryogenically cooled Si(111)
211 channel-cut monochromator to an energy of 12 keV with a flux of $\sim 1.1 \times 10^{10}$ photon/s. A
212 Kirkpatrick-Baez mirror pair was used to focus the incident beam to 700 × 530 nm
213 (hor × ver). The Maia detector uses a large detector array in backscatter geometry to
214 maximize detected signal and count-rates for efficient imaging. Maia enables high overall
215 count-rates and uses an annular detector geometry, where the beam passes through the
216 detector and strikes the sample at normal incidence (Kirkham et al. 2010; Siddons et al.
217 2014). This enables a large solid-angle (~ 1.2 steradian) to be achieved in order to either
218 maximize detected signal or to reduce the dose and potential damage to a specimen (Ryan et

219 al. 2010; 2014). We first conducted a quick ‘survey scan’ (50–100 μm with a dwell time of
220 1–2 ms, taking 5–10 min. in total) to select the precise scan area. Then a ‘detailed scan’ was
221 conducted (resolution of 2–10 μm and a dwell time of 8–20 ms, taking 60–180 min. in total).

222
223 The live samples were prepared on-site immediately prior to scanning at beamline P06. The
224 samples were hand cut with a stainless-steel razor blade (‘dry knife’) and analysed within 10
225 minutes after excision. The fresh and freeze-dried samples were mounted between two sheets
226 of Ultralene thin film (4 μm) stretched over a Perspex frame magnetically attached to the
227 horizontal-vertical motion stage at atmospheric temperature ($\sim 20^\circ\text{C}$). The possibility of
228 radiation-induced damage in μXRF analysis (especially in fresh/hydrated samples) is an
229 important consideration that may limit the information sought from the analysis (van der Ent
230 et al. 2017b). In a recent study, radiation dose limits for μXRF analysis were assessed, and in
231 hydrated plant tissue dose-limits are 4.1 kGy before detectable damage occurs (Jones et al.
232 2019). To limit radiation damage, we used a fast scanning (per-pixel dwell time is less than
233 10 ms, and hence effective radiation dose is low).

234
235 **2.7 Data processing and statistics** – The XRF event stream was analysed using the Dynamic
236 Analysis method (Ryan and Jamieson 1993; Ryan 2000) as implemented in GeoPIXE (Ryan
237 et al. 1990; 2005). The matrix file used for the spectra fitting was an assumed freeze-dried
238 plant material composition of $\text{C}_{31}\text{O}_{15}\text{H}_{51}\text{N}_2\text{S}_{0.8}$ with a density of 0.75 g cm^{-3} , and for
239 live/fresh samples the composition was $\text{C}_{7.3}\text{O}_{33}\text{H}_{59}\text{N}_{0.7}\text{S}_{0.8}$ with a density of 0.90 g cm^{-3} and
240 considering two layers of Ultralene (4 μm).

241 242 **3. RESULTS**

243
244 **3.1 Soil chemistry in the habitat of the five species** – Most of the Soils originated from
245 non- (Rivière-Bleue) or only moderately serpentinised (Monts des Koghis) peridotite and
246 were moderately weathered (*i.e.* they have full or partial ferralitic properties). The range of
247 soil pH values was quite narrow around pH 6.0 (pH 5.8–6.2) except for the soils hosting
248 *Psychotria gabriellae*, which were more acidic ($< \text{pH } 5.5$) than the other soils (Table 1).
249 Total Fe ranged from 128–388 mg Fe g^{-1} with most around 300 mg Fe g^{-1} and total Al from
250 12.2–42.5 mg Al g^{-1} . Soils had high Mg concentrations from 5.2–20.1 mg Mg g^{-1} and
251 depleted concentrations of Ca. All soils were extremely depleted in total K with most values
252 around 200 $\mu\text{g g}^{-1}$ and none exceeded 1000 $\mu\text{g g}^{-1}$. Furthermore, P total concentrations were

253 very low (from 280–780 $\mu\text{g P g}^{-1}$), as were S total concentrations (590–1200 $\mu\text{g S g}^{-1}$). Total
254 Co, Cr, Mn, and Ni concentrations reflected typical values from ferralic ultramafic soils:
255 340–1080 $\mu\text{g Co g}^{-1}$, 339–1080 $\mu\text{g Cr g}^{-1}$, 2880–7280 $\mu\text{g Mn g}^{-1}$, and 2.7–10.5 mg Ni g^{-1}
256 (Table 1).

257

258 Metal availability was assessed by both $\text{Sr}(\text{NO}_3)_2$ and DTPA extractions (Table 1). The
259 former provides a good picture of exchangeable ions retained by the soil Cation Exchange
260 Capacity (CEC), whereas DTPA extracts the isotopically-exchangeable pool, *i.e.* the Ni pool
261 that supplies hyperaccumulators and non-hyperaccumulators (Echevarria et al. 1998, 2006;
262 Massoura et al. 2005; Estrade et al. 2015). The $\text{Sr}(\text{NO}_3)_2$ exchangeable Ni in all soils ranged
263 from 6.4–38 $\mu\text{g Ni g}^{-1}$. Moreover, DTPA-extractable Ni was very high in all sampled soils. It
264 varied from 300–627 $\mu\text{g Ni g}^{-1}$ with no apparent difference between plant species. One soil
265 (*P. gabriellae* from Monts des Koghis) had exchangeable Co that was remarkably high (*i.e.*
266 8 $\mu\text{g Co g}^{-1}$) and exchangeable Mn was also highly available (*i.e.* 285 $\mu\text{g Mn g}^{-1}$). In the case
267 of DTPA-extractable Co, it was noticeable that most of the soils had similar concentrations,
268 limited between 49–78 $\mu\text{g Co g}^{-1}$; which appears higher than in typical ultramafic soils
269 (Echevarria, 2018; van der Ent et al. 2018a). For other metals, exchangeable concentrations
270 were limited in all soils and within expected values.

271

272 **3.2 Elemental profiles of the five species**

273 Bulk elemental concentrations of major trace elements were obtained for different parts of the
274 plant for the five taxa (Tables 2 & 3) and described below.

275

276 **Roots** – It is not practically possible to entirely clean roots from soil particle contamination.
277 Soil particles, and in particular nanometric or submicrometric particles, may be embedded
278 and cannot be entirely removed by rigorous washing or brushing. However, some stable
279 elements which are very unlikely to be taken up in large quantities by roots (*e.g.* Cr, Fe) help
280 to detect soil contamination. Typically, K was low in the roots (<2460 $\mu\text{g K g}^{-1}$) and
281 preferentially transferred in the leaves: all three species contained more than 1 Wt.% K in
282 leaves. A similar pattern was seen for Ni with highly enhanced translocation to the leaves:
283 (<3.41 mg Ni g^{-1} in roots of all three species whereas it reached 3.2 mg Ni g^{-1} in leaves).

284

285 **Bark** – In the bark samples of *G. pruinosa* var. *pruinosa* and *H. francii*, Ca was extremely
286 enriched (16 and 25 mg Ca g^{-1} respectively), whereas for *H. austrocaledonicus* and *P.*

287 *acuminata*, Ca content was in the same range as in all other parts. The bark (including
288 phloem) had very high concentrations of Ni in *H. austrocaledonicus* (up to 48.5 mg Ni g⁻¹),
289 and in *P. acuminata* (up to 10 mg Ni g⁻¹). On the contrary, *G. pruinosa* var. *pruinosa* and *H.*
290 *francii* had very low Ni concentrations (410 and 920 µg Ni g⁻¹ respectively) in the bark.

291

292 **Stem tissues (without bark)** – Similarly to the bark, Ni concentrations were low in the
293 branches of both *G. pruinosa* var. *pruinosa* and *H. francii*. They were intermediate in *H.*
294 *austrocaledonicus* and *P. acuminata* and high in *P. gabriellae* (>15 mg Ni g⁻¹) (data not
295 shown).

296

297 **Leaf tissues (whole leaf)** – Foliar Ca concentrations (Table 2) were typically five-fold higher
298 than in the soils, in contrast to the extremely high soil Mg concentrations that had been
299 effectively limited from uptake. All species except *G. pruinosa* var. *pruinosa* reached
300 extremely high K concentrations in leaves (sometimes >10 mg K g⁻¹) in comparison to soil
301 concentrations ranging from 224–864 µg K g⁻¹ (Table 1). The maximum foliar K
302 concentration for *G. pruinosa* var. *pruinosa* remained in the lower range compared to other
303 species (Table 2), but it was still five times more than the total K in the soil. Even though soil
304 S concentrations were low (<1200 µg S g⁻¹), foliar concentrations were remarkably high
305 reaching up to 8320 µg S g⁻¹ in the leaves. All five species are hypernickelophores (although
306 the maximum value in this study for *Homalium francii* was 9480 µg Ni g⁻¹) (Table 3, Fig. 3),
307 and Ni concentration values were consistent with earlier reports for these species (Jaffré et al.
308 1974; Reeves 2003; Jaffré et al. 2013). Although Co foliar concentrations were highly
309 variable for a given species, *H. francii* and *H. austrocaledonicus* reached values ≥120 µg Co
310 g⁻¹. Manganese concentrations of the five species in leaves were comparatively low (28–120
311 µg Mn g⁻¹), given the high available Mn concentrations in the soils (571–1090 µg Mn g⁻¹
312 DTPA-extractable Mn).

313

314 **Reproductive organs (flowers, fruits and seeds)** – Flowers of *P. gabriellae* were highly
315 enriched in Ni, contrary to those of *G. pruinosa* var. *pruinosa* (Table 3). The fruits (*i.e.*
316 pericarp, except for *P. gabriellae* as the endocarp surround the seed) were also strongly
317 enriched in Ni in both *P. acuminata* (mean of 6130 µg Ni g⁻¹) and *P. gabriellae* (mean of
318 9810 µg Ni g⁻¹) but relatively low in *G. pruinosa* var. *pruinosa* (1510 µg Ni g⁻¹).
319 Concentrations of other transition metals (*i.e.* Co, Cr, Mn, Zn) in fruits were remarkably low
320 in comparison with those of Ni. Seeds of *P. acuminata* (seed *stricto sensu*) and *P. gabriellae*

321 (seed *stricto sensu* surrounded by the endocarp *i.e.* pyrene) contained less Ni than the fruits
322 (or flowers in case of *P. gabriellae*), with high range values (4110 and 5420 $\mu\text{g Ni g}^{-1}$ Ni
323 respectively). The mesocarp of *P. acuminata* exuded green latex when sliced, suggesting high
324 Ni concentration in this seed.

325 **Latex of *Pycnandra acuminata*** – Samples of latex collected from the trunks of *P. acuminata*
326 in Rivière Bleue had a bright turquoise colour (Fig. 1f). The latex contained noticeable
327 concentrations of Ca that exceeded 10 mg Ca g^{-1} and were always more than 10 times higher
328 than Mg concentrations (Table 2). It contained some K (1140–3800 $\mu\text{g K g}^{-1}$) and Na (1560–
329 3320 $\mu\text{g Na g}^{-1}$), with all other major elements showing concentrations below 1200 $\mu\text{g g}^{-1}$. It
330 contained surprisingly high concentrations of Al (mean concentration of 810 $\mu\text{g Al g}^{-1}$ with
331 one value around 1500 $\mu\text{g Al g}^{-1}$) and Zn (mean concentration of 800 $\mu\text{g Zn g}^{-1}$). As expected
332 (Sagner et al. 1998; Perrier et al. 2004; Schaumlöffel et al. 2003; Callahan et al. 2008), Ni
333 concentrations were extremely high and ranged from 110–150 mg Ni g^{-1} . However, Co
334 concentrations in the latex were relatively low (mean of 41 $\mu\text{g Co g}^{-1}$) compared to Ni
335 concentrations. The Ni/Co ratio in latex was approximately 325, whereas it was
336 approximately 10 in the soil DTPA extract.

337

338 **Elemental distribution in whole leaf fragments** – Potassium was highly concentrated in the
339 midrib of all species except *P. gabriellae* (Fig. 4). It was also localised in the secondary veins
340 for *H. austrocaledonicus* and *G. pruinosa* var. *pruinosa* and had a high background
341 concentration throughout the leaves of *H. austrocaledonicus* but not *G. pruinosa* var.
342 *pruinosa*. In *P. gabriellae* there was a strong enrichment of K in minor veins whilst in *H.*
343 *francii*, K was enriched in the lamina surrounding the secondary veins. Alternatively, K was
344 depleted in the area surrounding the midrib of *P. acuminata* but was somewhat enriched at
345 the base of the secondary veins and depleted towards the outer ends.

346

347 There was no notable enrichment of Ca in the leaves of *P. gabriellae* (Fig. 4). In the other
348 species Ca was mainly concentrated in major veins and appears as small Ca-oxalate crystals
349 (small dots). In *G. pruinosa* var. *pruinosa* and *P. acuminata* these crystals underlined the
350 structure of minor veins order; whereas in *H. austrocaledonicus* and *H. francii* they were
351 more scattered throughout the leaf blade. Ca was totally absent in the veins of *H.*
352 *austrocaledonicus* but homogeneously distributed throughout the leaf blade.

353

354 In all species, Ni was strongly concentrated in the midveins and secondary veins except *P.*
355 *acuminata*, where Ni was concentrated in laticifers (Fig. 5). In *H. austrocaledonicus* and in
356 *G. pruinosa* var. *pruinosa* Ni was also highly concentrated in the minor veins order. That was
357 not the case for *H. francii* and *P. gabriellae*, for the latter there was also a notable enrichment
358 of Ni in the immediate surroundings of the main veins. In *P. acuminata*, Ni had a peculiar
359 distribution. It was mainly distributed along a network of elongated cellular structures
360 (laticifers) that were not part of the vascular system, unlike Ca or K that clearly highlighted
361 the vascular system. Manganese was co-localized with Ni in the veins of *H. francii*, but it had
362 a different distribution than Ni in *G. pruinosa* var. *pruinosa* (Fig. 5) as it was mainly
363 localised in the midrib and absent from all secondary and minor veins in this species. It was,
364 however, highly enriched in the surrounding areas of the midrib and the secondary vein.
365 Cobalt in *H. austrocaledonicus* and *P. acuminata* is co-localized with Ni throughout the leaf,
366 although at much lower concentrations.

367

368 Images and anatomical sections of the actual scanned freeze-dried samples are provided in
369 Suppl. Info (Fig. 4, 5). It should be noted that the concentrations of all elements appeared
370 higher in the midvein and leaf margins (that are curved inwards in *H. austrocaledonicus*) due
371 to greater thickness of these regions (hence generating more fluorescence X-rays). To a lesser
372 extent, this was also true for the secondary veins that are slightly thicker than the rest of the
373 leaf blade. While Ni concentrations appeared to be very high in the midribs of *P. gabriellae*
374 and *P. acuminata*, the cross sections (Fig. 7) revealed that Ni is in fact equally distributed in
375 the epidermis of midrib and lamina.

376

377 **3.3 Comparison of fresh/live leaves and freeze-dried leaf fragments**

378 There appeared to be differences in the leaf K distribution of *G. pruinosa* var. *pruinosa*
379 between freeze-dried and fresh material (Fig. 4 and 6). In freeze-dried material, K was mainly
380 distributed in the vascular system of the leaf: in the mid-rib and secondary veins. In the fresh
381 leaf, it seemed to be absent from all vascular tissues and concentrated in cell clusters in the
382 leaf lamina. With *P. gabriellae*, K in fresh samples was higher in the midrib, whereas it was
383 mostly located in secondary veins and almost absent from the mid-rib in freeze-dried leaves.
384 The distribution of Ni was generally similar (higher concentration in the mid-rib) in fresh and
385 freeze-dried material for both species.

386

387 **Elemental distribution in leaf midribs** – As the concentrations of all elements were
388 apparently higher in the leaf midrib (but refer to earlier notes about the effect of sample
389 thickness on XRF signal), a more detailed scan of these tissues was undertaken on cross-
390 sectioned fresh material for two species (*P. gabriellae* and *P. acuminata*, Fig. 7). In *P.*
391 *gabriellae*, K was present at high concentrations in all the tissues except in the epidermis.
392 Potassium appeared to be located also in the vacuoles of most of the cells. In *P. acuminata*, K
393 was also present in high concentration throughout the midrib, and was particularly rich in the
394 parenchyma, K concentrations were much lower in the vascular system and almost depleted
395 in the sclerenchyma surrounding vascular bundle.

396

397 Calcium was much less concentrated in midrib of both species. In *P. gabriellae* it appeared as
398 small localised patches principally distributed in the parenchyma. These patches were Ca-
399 oxalate crystals. In *P. acuminata*, Ca seemed to be only present in the adaxial epidermis of
400 the midrib and not anywhere else. Nickel and Mn seemed to be clearly co-localised in the
401 epidermis of both species. In *P. gabriellae*, both abaxial and adaxial epidermal cell layers
402 contained the highest concentrations of both elements with Mn concentrations higher in the
403 leaf blade epidermal tissues. However, in *P. acuminata*, only the adaxial epidermis had the
404 highest Ni concentrations while Mn concentrations were intermediate to high in both
405 epidermal tissues. In this species, very few hotspots with very high Ni concentrations also
406 appeared in parenchyma and collenchyma (Fig. 7).

407

408 **Elemental distribution in leaf petioles** – Petiole sections were examined as fresh samples
409 for *G. pruinosa* var. *pruinosa*, *P. gabriellae* and *P. acuminata* and as freeze-dried samples for
410 *H. francii* (Fig. 8 and 9). In all species K concentration was high in the cortex and phloem but
411 occurred in much lower concentration in the xylem (Fig. 8). However, in *P. gabriellae* and *P.*
412 *acuminata*, high K concentrations were notable in xylem rays. K concentration in the
413 epidermis varied between species, with particularly high concentrations in *G. pruinosa* var.
414 *pruinosa*. Calcium distribution was similar to K, but with lower concentrations in addition to
415 low concentrations of Ca in epidermal cells. Note that Ca appeared as small dots in the form
416 of Ca-oxalate.

417

418 Nickel in *G. pruinosa* var. *pruinosa* and *P. gabriellae* was located in the epidermis of the
419 petiole with lower, but non-negligible, concentrations in the outer cortex of *P. gabriellae*
420 (Fig. 9). In *H. francii*, the reverse was observed, and Ni was mostly concentrated in the inner

421 part (parenchyma) and absent from the epidermis and the vascular bundle. In *P. acuminata*, a
422 few large patches of high Ni concentration occurred randomly in the parenchyma, and small,
423 but more regular, patches were observed in the adaxial epidermis of the petiole (the flatter
424 part in the two sections). These large Ni patches were interpreted as leaking laticifers after
425 sectioning of the fresh petiole. In *H. francii*, Zn was located in similar areas as Ni but at
426 lower concentrations. Manganese in *G. pruinosa* var. *pruinosa* and *P. gabriellae* was only
427 concentrated in the epidermis of the petiole.

428

429 **Elemental distribution in fresh stem sections of *Psychotria gabriellae*** – In stem sections,
430 the K concentrations were highest in the epidermis and progressively decreased towards the
431 vascular tissues (Fig. 10). High concentrations, though much lower than in the epidermis,
432 were also found in phloem tissues, pith and in the inner part of xylem tissues. Calcium was
433 ubiquitous in the stem as localised Ca-oxalate particles, except in the xylem tissues. The
434 distribution pattern of Ni was clearly similar to that of K in stems. Nickel was even more
435 pronouncedly enriched in the epidermal cell layer than K.

436

437 **Cell-level elemental distribution in *Psychotria gabriellae*** – High-resolution scans (0.5 μm)
438 of a fresh/live hand-cut leaf blade of *P. gabriellae* were obtained (Fig. 11). The abaxial
439 epidermis of this species contains two layers of large cells whereas the adaxial epidermis had
440 only one layer (Fig. 11). Potassium was enriched in the mesophyll and highly enriched in the
441 vacuoles of the abaxial epidermal cells. In contrast, Ca was strongly depleted in the vacuoles
442 of these cells and only detectable in epidermal cell walls, but it formed localized Ca fibres
443 (raphides of Ca-oxalate precipitates) in the spongy mesophyll. The distribution of Mn and Co
444 was rather similar to each other. Both elements were concentrated in the vacuoles of the
445 adaxial epidermal cells. Zinc was slightly enriched in the spongy mesophyll. Nickel was
446 extremely enriched in the vacuoles of the adaxial epidermal cells and to a lesser extent in the
447 vacuoles of the outer layer of abaxial epidermal cells. It also appeared to be present in the
448 apoplastic space between the inner layer cells of the abaxial epidermis. It was notably low in
449 the palisade mesophyll.

450

451 **4. DISCUSSION**

452

453 **4.1 Soil-plant interactions and elemental uptake**

454 While most Ni hyperaccumulators worldwide have been described from serpentinite soils
455 (*i.e.* soils derived from serpentinite minerals characterised by very high Mg/Ca, very low K
456 and high pH, see Echevarria 2018), in New Caledonia hyperaccumulation also occurs on non-
457 serpentinitised peridotites. The high diversity of soils derived from ultramafic rocks is an
458 important pedological feature of New Caledonia, ranging from magnesium-rich brown soils
459 (*e.g.* Cambisols) to impoverished Fe-rich soils (*e.g.* Ferralsols) (Jaffré 1976; Isnard et al.
460 2016). All of the studied species reach the status of hypernickelophore (plant with >10 mg Ni
461 g⁻¹); which may be partly explained by the high availability of Ni in all of the soil samples.
462 This is mainly due to two processes; in the case of Monts des Koghis, soil erosion rejuvenates
463 ultramafic properties of the ferrallic material in the soils (van der Ent et al. 2018a), thus
464 keeping exchangeable Mg and Ni at high concentrations with some contribution of moderate
465 laterization. In the case of Rivière Bleue, the alluvial conditions and temporary waterlogging
466 likely contribute to the dissolution of Ni-bearing Fe-oxyhydroxides, thus releasing substantial
467 amounts of available Ni (Antić-Mladenović et al. 2011). Forest areas over peridotite humus-
468 rich alluvium are Ni-rich and host the famous *P. acuminata* (Jaffré et al. 1976) and other
469 hyperaccumulators (*H. austrocaledonicus*, *H. guillainii*, *P. gabriellae*) (Jaffré and Schmid
470 1974).

471
472 For major elements, four species out of five had notably high K concentrations reaching
473 almost 10 mg K g⁻¹ in leaves except in *G. pruinosa* var. *pruinosa* (typically 2000 µg K g⁻¹).
474 These concentrations are high for K-impoverished ultramafic soils (mean for K for 146
475 species in forest on ultramafic soils is 8.6 mg K g⁻¹), compared to plants growing on non-
476 ultramafic soils (Jaffré 1980). The low Ca concentration in the soil and low Ca/Mg quotient
477 contributes to the edaphic stresses on ultramafic soils (Proctor 2003). In New Caledonia,
478 exchangeable Ca²⁺ are very low while Mg concentration are extremely high leading to very
479 low Ca/Mg quotient on serpentinite (Jaffré 1976) and also on peridotite in this study. The
480 Ca/Mg quotient in leaves of all five species is high and closer to 1 (with the exception of *H.*
481 *austrocaledonicus*). The ability for preferential Ca over Mg uptake is characteristic for many
482 ultramafic species (Brady et al. 2005; Brearley 2005), including Ni hyperaccumulators (Bani
483 et al. 2007; van der Ent et al. 2018a).

484
485 Potassium and phosphorus are the most limiting nutrients in tropical ultramafic soils (Proctor
486 2003), where they have been leached or strongly bound to Fe oxides. Nickel
487 hyperaccumulators efficiently take up these elements and significantly contribute to their

488 biogeochemical cycling in ultramafic soils (Echevarria 2018). The association between Ni
489 and nutrient assimilation remain unknown, though it has been suggested that extensive uptake
490 of Ni is the result of root foraging and assimilation of essential nutrients that are depleted in
491 the soils. Another explanation would be that Ni accumulation slows down plant development
492 leading to stunted habit and greater uptake/accumulation of nutrients (Brooks et al. 1974).
493 Sulphate is typically the dominant anion in ferralic ultramafic soils; therefore, it is not
494 surprising that it is co-accumulated where cations are highly accumulated within the plant to
495 ensure ionic balance.

496

497 In the case of Co, the foliar concentrations are sometimes high and associated with a high
498 DTPA-Co/DTPA-Ni quotient in the soil. The Co availability is probably also enhanced
499 during temporary reduction events in alluvial soils from Rivière Bleue (where four out the
500 five studied species were sampled). Similar results have been reported for a tropical Ni-Co
501 hyperaccumulator plant (*Glochidion cf. sericeum*) from Borneo where unusually high Co
502 uptake is linked to temporary waterlogged ultramafic soils (van der Ent et al. 2018c).

503

504 **4.2 Latex of *Pycnanandra acuminata***

505 Citrate is the main chelating agent of Ni in the latex of *P. acuminata* (Lee et al. 1978;
506 Schaumlöffel et al. 2003; Callahan et al. 2008). However, citrate complexes have much
507 higher stability constants (log K_1 values) with trivalent ions such as Al than with Ni, typical
508 values for 1:1 complexes are reported to be 10.2, 4.8 and 4.5 for Al, Ni and Zn respectively
509 (more than 10^5 times more stable than the Ni-citrate complex) (Martell et al. 2004; Cardiano
510 et al. 2017). This may explain why we observed such high Al concentrations in the latex
511 despite the low availability of soil Al. Zinc, which is more available than Al, was also high in
512 the latex because it has a stability constant similar to Ni. High Al uptake and transfer by
513 laticifers, while in low concentration in branches, fruits and seeds, is possibly an indication
514 that this network loads metals including Ni from the root up to all other plant parts
515 independently from the vascular system (van der Ent et al. unpublished).

516

517 **4.3 Effects of freeze-drying on elemental distribution**

518 Scattering of X-rays by water reduces XRF signal, meaning that less signal from hydrated
519 samples (live samples) is detected. Furthermore, this effect is more pronounced with low
520 fluorescence energy (e.g. K). Quite the opposite, freeze-drying increases the apparent
521 concentration of an element by removing the solute. Calcium is present as Ca-rich deposits,

522 presumably Ca-oxalate crystals (Franceschi and Nakata 2005), and as a consequence is not
523 impacted by the water loss during freeze-drying. Given that K is the most mobile cation in
524 plant tissues, it is likely to be more affected by the movement of water upon freeze-drying.
525 There are several lines of evidence that show that freeze-drying does modify the distribution
526 of elements at micro-scale (Tylko et al. 2006; Wang et al. 2013). This study is the first to
527 report extensive μ XRF observations of fresh plant samples allowing the analysis of larger
528 surfaces than for frozen-hydrated samples which need to be constantly maintained under a
529 cold stream of N₂ gas (typically able to keep a sample area < 2 mm diameter wide frozen).

530

531 **4.4 Patterns of Ni hyperaccumulation and other elements**

532 The tissue-level and cellular-level distribution of Ni in the epidermal cells in *P. gabriellae*, *H.*
533 *austrocaledonicus*, and *H. francii* conforms with the majority of studied Ni hyperaccumulator
534 plant species globally, including (temperate) herbaceous species (see e.g. Broadhurst et al.
535 2004) and (tropical) woody plants (see van der Ent et al. 2017a,b). However, two of the
536 studied species (*G. pruinosa* var. *pruinosa* and *P. acuminata*) have distinctive patterns in
537 their Ni tissue-level distribution from what has been observed so far in other species. *Geissois*
538 *pruinosa* var. *pruinosa* accumulates high Ni but much less potassium than all the other
539 species (K hyperaccumulation is a general feature among all Ni hyperaccumulators globally).
540 In fact, K and Ni appear to have inverse foliar distribution in *G. pruinosa* var. *pruinosa*
541 whereas they typically co-accumulate in other species (e.g. *P. gabriellae*).

542

543 Nickel is associated in tissues adjacent to vascular bundles in the epidermal tissues (and/or
544 cortex); within vacuoles and apoplastic space in cell walls. When there is a lower Ni
545 concentration it is only seen in the cell walls, but if there is a higher concentration it is
546 observed in both the cell walls and in the vacuoles. That could mean that the preferred
547 localisation for Ni storage is apoplastic space, only the extreme levels of hyperaccumulation
548 would require active uploading into the vacuoles. The local distribution of Mn and Co are
549 usually identical to that of Ni, inferring that co-accumulation could be due to the same
550 transport pathways. However, the distribution of Zn is dissimilar to Ni, except for in *P.*
551 *gabriellae*, and this mirrors the findings in the tropical Ni-Zn hyperaccumulator
552 *Dichapetalum gelonioides* (Nkrumah et al. 2018).

553

554 **5. CONCLUSIONS**

555 Many tropical hyperaccumulator species have extraordinarily high Ca concentrations
556 compared to prevailing soils concentrations (van der Ent and Mulligan 2015). Correlations
557 between Ca and Ni have been reported in the leaves of *Hybanthus floribundus* from Australia
558 (Farago and Mahmoud 1983). Here we report high Ca concentration in leaves, branches and
559 bark, probably associated with calcium oxalate crystals deposited in epidermis and cortex
560 (and pith in *P. gabriellae*). Calcium oxalate formation is a general mechanism for regulating
561 bulk-free Ca²⁺ level in tissues and organs. It can also have a support function when located
562 in the sclerenchyma. For *P. acuminata*, the high Ca contents in the abaxial cortex of petioles
563 and midribs suggests that it has a role in reinforcing the structure of these long petioles. In *P.*
564 *acuminata*, Ca is present in vascular bundles, also probably as Ca-oxalate crystals, and acts as
565 a component of their structures. Nickel and Ca are proxies for two different and disconnected
566 networks in this plant, the former for laticifers and the latter for the vascular system.

567

568 The laticifers constitute an independent network of cells that operate in parallel to the
569 vascular systems (xylem and phloem) and is the main sink for Ni. Although the epidermal
570 layer of *P. acuminata* leaves has been reported to be rich in Ni (Perrier et al. 2004), SEM-
571 EDS used in that study only probed to a maximum depth of 5 µm and hence was unable to
572 reveal laticifers. Because it has a greater penetration depth (>1000 µm for hydrated biological
573 samples) synchrotron µXRF using hard X-rays (incident energy >8 keV) allows direct
574 observation of the unique distribution of Ni in *P. acuminata*. Nickel is mostly present in
575 laticifers and transported throughout the whole tree from roots to leaves. The occurrence of
576 these Ni-rich laticifers is a specific phenomenon that has not been visualized with µXRF in
577 other species to date. Laticifers are impossible to section without their destruction because
578 they are pressurized (Pickard 2008). Consequently, physical sectioning of laticifers causes
579 them to expel their contents, resulting in Ni spills. In order to visualise laticifers, non-
580 destructive techniques such as synchrotron X-ray fluorescence tomography (µXRF-CT) are
581 required (de Jonge and Vogt 2010; Lombi et al. 2011; van der Ent et al. 2017b), and intact
582 laticifers can be readily observed in large maps of intact tissues.

583

584 **Acknowledgements**

585 The authors thank the Province Sud de Nouvelle-Calédonie for permission to collect the plant
586 material samples (permits 1503-2016/ARR/DENV and 1206-2018/ARR/DENV), and S.
587 Palermo for access to Monts des Koghis. This research was undertaken at P06 at DESY, a
588 member of the Helmholtz Association (HGF). The research leading to this result has been

589 supported by the project CALIPSOplus under the Grant Agreement 730872 from the EU
590 Framework Programme for Research and Innovation HORIZON 2020. A. van der Ent was
591 the recipient of a Discovery Early Career Researcher Award (DE160100429) from the
592 Australian Research Council. V. Gei was the recipient of an Australia Awards PhD
593 Scholarship from the Australian Federal Government.

594

595

596 **REFERENCES**

597

598 Adıgüzel N, Reeves RD (2012) Important serpentine areas of Turkey and distribution
599 patterns of serpentine endemics and nickel accumulators. *Bocconea* 24:7–17.

600

601 Andresen E, Peiter E, Küpper H (2018) Trace metal metabolism in plants. *Journal of*
602 *Experimental Botany* 69(5):909–954.

603

604 Antić-Mladenović S, Rinklebe J, Frohne T, Stärk H-J, Wennrich R, Tomić Z, Ličina V
605 (2011) Impact of controlled redox conditions on nickel in a serpentine soil. *Journal of*
606 *Soils and Sediments* 11(3):406–415.

607

608 Bani A, Echevarria G, Sulçe S, Morel JL, Mullai A (2007) In-situ phytoextraction of Ni by a
609 native population of *Alyssum murale* on an ultramafic site (Albania). *Plant Soil*
610 293(1–2):79–89.

611

612 Bhatia NP, Orlic I, Siegele R, Ashwath N, Baker AJM, Walsh KB (2003) Elemental mapping
613 using PIXE shows the main pathway of nickel movement is principally symplastic
614 within the fruit of the hyperaccumulator *Stackhousia tryonii*. *New Phytologist*
615 160:479–448.

616

617 Bhatia NP, Walsh KB, Orlic I, Siegele R, Ashwath N, Baker AJM (2004) Studies on spatial
618 distribution of nickel in leaves and stems of the metal hyperaccumulator *Stackhousia*
619 *tryonii* Bailey using nuclear microprobe (micro-PIXE) and EDXS techniques.
620 *Functional Plant Biology* 31(11):1061–1074.

621

622 Becquer T, Bourdon E, Pétard J (1995) Disponibilité du nickel le long d'une toposéquence de
623 sols développés sur roches ultramafiques de Nouvelle-Calédonie. *Comptes Rendus de*
624 *l'Académie des Sciences Série 2a* 321:585–592.

625

626 Berazaín R, de la Fuente V, Rufo L, Rodríguez N, Amils R, Díez-Garretas B, Sánchez-Mata
627 D, Asensi A (2007) Nickel localization in tissues of different hyperaccumulator
628 species of Euphorbiaceae from ultramafic areas of Cuba. *Plant Soil* 293(1):99–106.

629

630 Bidwell SD, Crawford SA, Woodrow IE, Sommer Knudsen J, Marshall AT (2004)
631 Subcellular localization of Ni in the hyperaccumulator, *Hybanthus floribundus*
632 (Lindley) F. Muell. *Plant, Cell & Environment* 27(6):705–716.
633

634 Brady KU, Kruckeberg AR, Bradshaw Jr. HD (2005) Evolutionary ecology of plant
635 adaptation to serpentine soils. *Annual Review of Ecology, Evolution, and Systematics*
636 36:243–266.
637

638 Brearley F (2005) Nutrient limitation in a Malaysian ultramafic soil. *Journal of Tropical*
639 *Forest Science* 17(4): (4):596–609.

640 Broadhurst CL, Chaney RL, Angle JS, Erbe EF, Mangel TK (2004) Nickel localization and
641 response to increasing Ni soil levels in leaves of the Ni hyperaccumulator *Alyssum*
642 *murale*. *Plant Soil* 265:225–242.
643

644 Broadhurst CL, Tappero RV, Mangel TK, Erbe EF, Sparks DL, Chaney RL (2009)
645 Interaction of nickel and manganese in accumulation and localization in leaves of the
646 Ni hyperaccumulators *Alyssum murale* and *Alyssum corsicum*. *Plant Soil*
647 314(1/2):35–48.
648

649 Brooks RR, Lee J, Jaffré T (1974) Some New Zealand and New Caledonia plant
650 accumulators of nickel. *Journal of Ecology* 62:493–499.
651

652 Brooks RR, Morrison RS, Reeves RDR, Dudley TRT, Akman YY (1979)
653 Hyperaccumulation of nickel by *Alyssum* Linnaeus (Cruciferae). *Proceedings of the*
654 *Royal Society of London. Series B* 203:387–403.
655

656 Brooks RR, Chambers MF, Nicks LJ, Robinson BH (1998) Phytomining. *Trends in Plant*
657 *Science* 3(9):359–362.
658

659 Brooks RR, Robinson BH (1998) The potential use of hyperaccumulators and other plants for
660 phytomining. In: Brooks RR ed. *Plants that hyperaccumulate heavy metals*.
661 Wallingford, Oxon, UK.: CAB International, 327–356.
662

663 Callahan DL, Roessner U, Dumontet V, Perrier N, Wedd AG, O’Hair RAJ, Baker AJM,
664 Kolev SD (2008) LC–MS and GC–MS metabolite profiling of nickel(II) complexes in
665 the latex of the nickel-hyperaccumulating tree *Sebertia acuminata* and identification
666 of methylated aldaric acid as a new nickel(II) ligand. *Phytochemistry* 69:240–251.
667

668 Cardiano P, Cigala RM, Crea F, Giacobello F, Giuffre O, Irto A, Lando G, Sammartano .
669 (2017) Sequestration of aluminium(III) by different natural and synthetic organic and
670 inorganic ligands in aqueous solution. *Chemosphere* 186:535–545.
671

672 Chaney RL (1983) Potential effects of waste constituents on the food chain. In: Parr JF,
673 Marsh PB, Kla JM eds. *Land treatment of hazardous wastes*. Park Ridge, NJ: Noyes
674 Data Corp, 152–240.
675

676 Chaney RL, Angle JS, Broadhurst CL, Peters CA, Tappero RV, Sparks DL (2007) Improved
677 understanding of hyperaccumulation yields commercial phytoextraction and
678 phytomining technologies. *Journal of Environmental Quality* 36(5):1429–1443.
679

680 Echevarria G, Morel J, Fardeau J, Leclerc-Cessac E (1998) Assessment of phytoavailability
681 of nickel in soils. *Journal of Environmental Quality* 27(5):1064–1070.
682

683 Echevarria G, Massoura ST, Sterckeman T, Becquer T, Schwartz C, Morel JL (2006)
684 Assessment and control of the bioavailability of nickel in soils. *Environmental*
685 *Toxicology and Chemistry* 25(3):643–651.

686 Echevarria G (2018) Genesis and behaviour of ultramafic soils and consequences for nickel
687 biogeochemistry. In: van der Ent A, Echevarria G, Baker AJM, Morel JL eds.
688 *Agromining: Farming for metals: extracting unconventional resources using plants:*
689 *Mineral Resources Reviews series*, Cham: Springer International Publishing, 135–
690 156.
691

692 Erskine PD, Lee G, Fogliani B, L’Huillier L, McCoy S (2018) Incorporating
693 Hyperaccumulator Plants into Mine Rehabilitation in the Asia-Pacific Region. In: Van
694 der Ent A, Echevarria G, Baker AJM, Morel JL, eds. *Agromining: extracting*
695 *unconventional resources from plants*. *Mineral Resource Reviews series*, Cham:
696 Springer International Publishing, 117–133.

697
698 Estrade N, Cloquet C, Echevarria G, Sterckeman T, Deng T, Tang Y, Morel JL (2015)
699 Weathering and vegetation controls on nickel isotope fractionation in surface
700 ultramafic environments (Albania). *Earth and Planetary Science Letters* 423:24–35.
701
702 Farago ME, Mahmoud IEDAW (1983) Plants that accumulate metals (Part VI): Further
703 studies of an Australian nickel accumulating plant. *Minerals and the Environment*
704 5(4):113–121.
705
706 Franceschi VR, Nakata PA (2005) Calcium oxalate in plants: formation and function. *Annual*
707 *Review of Plant Biology* 56: 41–71.
708
709 Gei V, Erskine PD, Harris HH, Echevarria G, Mesjasz-Przybyłowicz J, Barnabas AD,
710 Przybyłowicz WJ, Kopittke PM, van der Ent A (2018) Tools for discovery of
711 hyperaccumulator plant species and understanding their ecophysiology. In: van der
712 Ent A, Echevarria G, Baker AJM, Morel JL, eds. *Agromining: Farming for Metals:*
713 *Extracting Unconventional Resources Using Plants*. Mineral Resource Reviews
714 series, Cham: Springer International Publishing, 117–133.
715
716 Gei V, Isnard S, Erskine PD, Echevarria G, Fogliani B, Jaffré T, van der Ent A (2020) A
717 systematic assessment of the occurrence of trace element hyperaccumulation in the
718 flora of New Caledonia. *Botanical Journal of Linnaean Society*. In Press.
719
720 Groeber S, Przybyłowicz W, Echevarria G, Montarges-Pelletier E, Barnabas A, Mesjasz-
721 Przybyłowicz J (2015) Fate of nickel and calcium in seedlings of the
722 hyperaccumulator *Berkheya coddii* during germination. *Biologia plantarum* 59(3):
723 560–569.
724
725 Hopkins HCF, Pillon Y, Hoogland R (2014) Cunoniaceae; Flore de la Nouvelle-Calédonie,
726 Vol 25 Muséum Paris, IRD Marseille 455pp.
727
728 Isnard S, L’Huillier L, Rigault F, Jaffré T (2016) How did the ultramafic soils shape the flora
729 of the New Caledonian hotspot? *Plant Soil* 403(1):53–76.
730

731 Jaffré T (1976) Composition chimique et conditions de l'alimentation minérale des plantes
732 sur roches ultrabasiques (Nouvelle Calédonie). Cah. ORSTOM Sér. Biol. 11.
733
734 Jaffré, T (1980) Étude écologique du peuplement végétal des sol dérivés de roches
735 ultrabasiques en Nouvelle Calédonie. Travaux et Documents de L'ORSTOM 124.
736 Paris: ORSTOM.
737
738 Jaffré T, Veillon JM (1990) Etude floristique et structurale de deux forêts denses humides sur
739 roches ultrabasiques en Nouvelle-Calédonie. Adansonia (3–4):243–273.
740
741 Jaffré T, Schmid M (1974) Ecophysiologie - Accumulation du nickel par une Rubiacée de
742 Nouvelle-Calédonie, *Psychotria douarrei* (G. Beauvisage) Däniker. Comptes Rendus
743 de l'Académie des Sciences, Paris, 278:1727–1730.
744
745 Jaffré T, Brooks RR, Lee J, Reeves RD (1976) *Sebertia acuminata*: A hyperaccumulator of
746 nickel from New Caledonia. Science 193: 579–580.
747
748 Jaffré T, Brooks RR, Trow JM (1979) Hyperaccumulation of nickel by *Geissois* species.
749 Plant Soil 51(1): 157–161.
750
751 Jaffré T, Pillon Y, Thomine S, Merlot S (2013) The metal hyperaccumulators from New
752 Caledonia can broaden our understanding of nickel accumulation in plants. Frontiers
753 in Plant Science 4(279):1–7.
754 Jaffré T, Reeves RD, Baker AJM, van der Ent A (2018) The discovery of nickel
755 hyperaccumulation in the New Caledonian tree *Pycnandra acuminata*: 40 years on.
756 New Phytologist 218:397–400.
757
758 Jones MWM, Kopittke PM, Casey L, Reinhardt J, Blamey FPC, van der Ent A (2019)
759 Assessing radiation dose limits for X-ray fluorescence microscopy analysis of plant
760 specimens. Ann Bot. doi.org/10.1093/aob/mcz195
761
762 de Jonge, MD, Vogt S (2010) Hard X-ray fluorescence tomography-an emerging tool for
763 structural visualization. *Current Opinion in Structural Biology* 20:606–614.
764

765 Kachenko AG, Singh B, Bhatia NP, Siegele R (2008) Quantitative elemental localisation in
766 leaves and stems of nickel hyperaccumulating shrub *Hybanthus floribundus* var.
767 *floribundus* using micro-PIXE spectroscopy. Nuclear Instruments and Methods in
768 Physics Research Section B: Beam Interactions with Materials and Atoms
769 266(4):667–676.
770

771 Kirkham R, Dunn PA, Kuczewski AJ, Siddons DP, Dodanwela R, Moorhead GF, Ryan CG,
772 De Geronimo G, Beuttenmuller R, Pinelli D, et al. (2010) The Maia spectroscopy
773 detector system: engineering for integrated pulse capture, low latency scanning and
774 real time processing. *AIP Conference Proceedings* 1234(1): 240–243.
775

776 Krämer U (2010) Metal Hyperaccumulation in Plants. Annual Review of Plant Biology
777 61(1):517–534.
778

779 Krämer U, Talke IN, Hanikenne M (2007) Transition metal transport. FEBS Letters 581:
780 2263-2272.

781 Kukier U, Chaney RL (2001) Amelioration of nickel phytotoxicity in muck and mineral soils.
782 Journal of Environmental Quality 30:1949–1960.

783 Küpper H, Lombi E, Zhao FJ, Wieshammer G, McGrath SP (2001) Cellular
784 compartmentation of nickel in the hyperaccumulators *Alyssum lesbiacum*, *Alyssum*
785 *bertolonii* and *Thlaspi goesingense*. Journal of Experimental Botany 51:2291–2300.

786 Lee J, Reeves RD, Brooks RR, Jaffré T (1978) The relation between nickel and citric acid in
787 some nickel-accumulating plants. Phytochemistry 17:1033–1035.
788

789 Lindsay WL, Norvell WA (1978) Development of a DTPA soil test for zinc, iron,
790 manganese, and copper. Soil Science Society of America Journal 42:421–428.
791

792 Lombi E, de Jonge MD, Donner E, Kopittke PM, Howard DL, Kirkham R, Ryan CG,
793 Paterson D (2011) Fast X-Ray fluorescence microtomography of hydrated biological
794 samples. PLoS ONE 6: e20626–5.
795

796 Losfeld G, Mathieu R, L'Huillier L, Fogliani B, Jaffré T, Grison C (2015a) Phytoextraction
797 from mine spoils: insights from New Caledonia. *Environmental Science and Pollution*
798 *Research* 22(8):5608–19.
799

800 Losfeld G, L'Huillier L, Fogliani B, Jaffré T, Grison C. 2015b. Mining in New Caledonia:
801 environmental stakes and restoration opportunities. *Environmental Science and*
802 *Pollution Research* 22(8): 5592–5607.
803

804 Martell AE, Smith RM, Motekaitis RJ. 2004. NIST Critically Selected Stability Constants of
805 Metal Complexes Database, 8.0. National Institute of Standard and Technology,
806 Gaithersburg, MD.
807

808 Massoura ST, Echevarria G, Leclerc-Cessac E, Morel JL (2005) Response of excluder,
809 indicator, and hyperaccumulator plants to nickel availability in soils. *Soil Research*
810 42(8):933–938.
811

812 McNear DH, Peltier E, Everhart J, Chaney RL, Sutton S, Newville M, Rivers M, Sparks DL
813 (2005) Application of quantitative fluorescence and absorption-edge computed
814 microtomography to image metal compartmentalization in *Alyssum murale*.
815 *Environmental Science & Technology* 39(7): 2210–2218.

816 Mesjasz-Przybyłowicz J, Balkwill K (1994) Proton microprobe and X-ray fluorescence
817 investigations of nickel distribution in serpentine flora from South Africa. *Nuclear*
818 *Instruments and Methods B* 89: 208–212.
819

820 Mesjasz-Przybyłowicz J, Balkwill K, Przybyłowicz WJ, Annegarn HJ, Rama DBK (1996a)
821 Similarity of nickel distribution in leaf tissue of two distantly related
822 hyperaccumulating species. In: van der Maesen LJG, van der Burgt XM, van
823 Medenbach de Rooy JM. *The Biodiversity of African Plants*. Wageningen, The
824 Netherlands: Springer: Dordrecht. 331–335.
825

826 Mesjasz-Przybyłowicz J, Przybyłowicz WJ, Prozesky VM, Pineda CA (1996b) Elemental
827 distribution in a leaf of *Senecio coronatus*. *Proceedings of the Microscopy Society of*
828 *Southern Africa* 26:68.
829

- 830 Mesjasz-Przybyłowicz J, Przybyłowicz WJ, Prozesky VM (1997a) Nuclear microprobe
831 investigation of Ni distribution in organs and cells of hyperaccumulating plants. In:
832 'The ecology of ultramafic and metalliferous areas': Proceedings of the second
833 international conference on serpentine ecology, pp. 223–224.
834
- 835 Mesjasz-Przybyłowicz J, Przybyłowicz WJ, Prozesky VM, Pineda CA (1997b) Quantitative
836 micro-PIXE comparison of elemental distribution in Ni-hyperaccumulating and non-
837 accumulating genotypes of *Senecio coronatus*. Nuclear Instruments and Methods in
838 Physics Research Section B: Beam Interactions with Materials and Atoms 130:368–
839 373.
840
- 841 Mesjasz-Przybyłowicz J, Przybyłowicz WJ, Rama DB, Pineda CA (1997c) Elemental
842 distribution in the Ni hyperaccumulator –*Senecio anomalous*. *Proceedings of the*
843 *Microscopy Society of Southern Africa* 27:89.
844
- 845 Mesjasz-Przybyłowicz J, Przybyłowicz WJ, Pineda CA (2001a) Nuclear microprobe studies
846 of elemental distribution in apical leaves of the Ni hyperaccumulator *Berkheya coddii*.
847 *South African Journal of Science* 97:591–592.
848
- 849 Mesjasz-Przybyłowicz J, Przybyłowicz WJ, Rama D, Pineda CA (2001b) Elemental
850 distribution in *Senecio anomalous*, a Ni hyperaccumulator from South Africa.
851 *South African Journal of Science* 97:593–595.
852
- 853 Mesjasz-Przybyłowicz J, Barnabas A, Przybyłowicz W (2007) Comparison of cytology and
854 distribution of nickel in roots of Ni hyperaccumulating and non-hyperaccumulating
855 genotypes of *Senecio coronatus*. *Plant Soil* 293:61–78.
856
- 857 Mesjasz-Przybyłowicz J, Przybyłowicz W, Barnabas A, van der Ent A (2016) Extreme nickel
858 hyperaccumulation in the vascular tracts of the tree *Phyllanthus balgooyi* from
859 Borneo. *New Phytologist* 209:1513–1526.
860
- 861 Nkrumah P, Van der Ent A, Echevarria G, Erskine PD (2018) Contrasting nickel and zinc
862 hyperaccumulation in subspecies of *Dichapetalum gelonioides* from Southeast Asia.
863 *Scientific Reports* 8: 9659.

864
865 Paul ALD, Gei V, Isnard S, Fogliani B, Echevarria G, Erskine PD, Jaffré T, Munzinger J, van
866 der Ent A (2020) Exceptional phloem nickel in *Hybanthus austrocaledonicus*
867 (Violaceae) from New Caledonia. *Annals of Botany*. In Press.
868
869 Perrier N, Colin F, Jaffré T, Ambrosi J-P, Rose J, Bottero J-Y (2004) Nickel speciation in
870 *Sebertia acuminata*, a plant growing on a lateritic soil of New Caledonia. *Comptes*
871 *Rendus Geoscience* 336(6):567–577.
872
873 Pickard WF (2008) Laticifers and secretory ducts: two other tube systems in plants. *New*
874 *Phytologist* 177: 877–888.
875
876 Pollard AJ, Powell KD, Harper FA, Smith JAC (2002) The genetic basis of metal
877 hyperaccumulation in plants. *Critical Reviews in Plant Sciences* 21:539–566.
878
879 Proctor J (2003) Vegetation and soil and plant chemistry on ultramafic rocks in the tropical
880 Far East. *Perspectives in Plant Ecology, Evolution and Systematics* 6(1):105–124.
881
882 Reeves RD (2003) Tropical hyperaccumulators of metals and their potential for
883 phytoextraction. *Plant Soil* 249:57–65.
884
885 Reeves RD, Baker AJM, Becquer T, Echevarria G, Miranda ZJG (2007) The flora and
886 biogeochemistry of the ultramafic soils of Goiás state, Brazil. *Plant Soil* 293(1):107–
887 119.
888
889 Reeves RD, Baker AJM, Jaffré T, Erskine PD, Echevarria G, van der Ent A (2018a) A global
890 database for hyperaccumulator plants of metal and metalloid trace elements. *New*
891 *Phytologist* 218:407–411.
892
893 Reeves RD, van der Ent A, Baker AJM (2018b) Global distribution and ecology of
894 hyperaccumulator plants. In: Van der Ent A, Echevarria G, Baker AJM, Morel JL,
895 eds. *Agromining: extracting unconventional resources from plants*. Mineral Resource
896 Reviews series, Cham: Springer International Publishing, 75–92.
897

898 Ryan C (2000) Quantitative trace element imaging using PIXE and the nuclear microprobe.
899 International Journal of Imaging Systems and Technology 11(4):219–230.
900

901 Ryan C, Cousens D, Sie S, Griffin W, Suter G, Clayton E (1990) Quantitative PIXE
902 microanalysis of geological material; using the CSIRO proton microprobe. Nuclear
903 Instruments and Methods in Physics Research Section B: Beam Interactions with
904 Materials and Atoms 47(1):55–71.
905

906 Ryan C, Jamieson D (1993) Dynamic analysis: on-line quantitative PIXE microanalysis and
907 its use in overlap-resolved elemental mapping. Nuclear Instruments and Methods in
908 Physics Research Section B: Beam Interactions with Materials and Atoms 77(1–
909 4):203–214.
910

911 Ryan C, Etschmann B, Vogt S, Maser J, Harland C, Van Achterbergh E, Legnini D (2005)
912 Nuclear microprobe–synchrotron synergy: Towards integrated quantitative real-time
913 elemental imaging using PIXE and SXRF. Nuclear Instruments and Methods in
914 Physics Research Section B: Beam Interactions with Materials and Atoms 231(1–
915 4):183–188.
916

917 Ryan CG, Siddons DP, Kirkham R, Dunn PA, Kuczewski A, Moorhead G, De Geronimo G,
918 Paterson DJ, de Jonge MD, Hough RM, *et al.* (2010) The new Maia detector system:
919 methods for high definition trace element imaging of natural material. AIP
920 Conference Proceedings 1221(1):9–17.
921

922 Ryan C, Siddons D, Kirkham R, Li Z, De Jonge M, Paterson D, Kuczewski A, Howard D,
923 Dunn P, Falkenberg G. *et al.* (2014) Maia X-ray fluorescence imaging: Capturing
924 detail in complex natural samples. Journal of Physics: Conference Series: IOP
925 Publishing. 012002.
926

927 Sagner S, Kneer R, Wanner G, Cosson J, Deus-Neumann B, Zenk M (1998)
928 Hyperaccumulation, complexation and distribution of nickel in *Sebertia acuminata*.
929 Phytochemistry 47:339–347.
930

931 Schaumlöffel D, Ouerdane L, Bouyssiére B, Łobiński R (2003) Speciation analysis of nickel
932 in the latex of a hyperaccumulating tree *Sebertia acuminata* by HPLC and CZE with
933 ICP MS and electrospray MS-MS detection. Journal of Analytical Atomic
934 Spectrometry 18:120–127.

935

936 Seregin IV, Kozhevnikova AD (2006) Physiological role of nickel and its toxic effects on
937 higher plants. Russian Journal of Plant Physiology 53(2):257–277.

938

939 Siddons D, Kirkham R, Ryan C, De Geronimo G, Dragone A, Kuczewski A, Li Z, Carini G,
940 Pinelli D, Beuttenmuller R, et al. (2014) Maia X-ray microprobe detector array
941 system. Journal of Physics: Conference Series: IOP Publishing. 012001.

942

943 Swenson U, Munzinger J (2010) Revision of *Pycnandra* subgenus *Sebertia* (Sapotaceae) and
944 a generic key to the family in New Caledonia. Adansonia 32(2):239–249.

945

946 Tappero R, Peltier E, Gräfe M, Heidel K, Ginder-Vogel M, Livi KJT, Rivers ML, Marcus
947 MA, Chaney RL, Sparks DL (2007) Hyperaccumulator *Alyssum murale* relies on a
948 different metal storage mechanism for cobalt than for nickel. New Phytologist
949 175:641–654.

950

951 Tylko G, Mesjasz-Przybyłowicz J, Przybyłowicz WJ (2006) X-ray microanalysis of
952 biological material in the frozen-hydrated state by PIXE. Microscopy Research and
953 Technique 70:55–68.

954

955 van der Ent A, Baker AJM, Reeves RD, Pollard AJ, Schat H (2012) Hyperaccumulators of
956 metal and metalloid trace elements: facts and fiction. Plant Soil 362(1):319–334.

957

958 van der Ent A, Baker A, Van Balgooy M, Tjoa A. 2013. Ultramafic nickel laterites in
959 Indonesia (Sulawesi, Halmahera): mining, nickel hyperaccumulators and
960 opportunities for phytomining. Journal of Geochemical Exploration 128:72–79.

961

962 van der Ent A, Baker AJM, Reeves RD, Chaney RL, Anderson CWN, Meech JA, Erskine
963 PD, Simonnot M-O, Vaughan J, Morel JL, et al. (2015a) Agromining: Farming for
964 metals in the future? Environmental Science & Technology 49(8):4773–4780.

965
966 van der Ent A, Erskine PD, Sumail S (2015b) Ecology of nickel hyperaccumulator plants
967 from ultramafic soils in Sabah (Malaysia). *Chemoecology* 25(5):243–259.
968
969 van der Ent A, Jaffré T, L'Huillier L, Gibson N, Reeves RD (2015c) The flora of ultramafic
970 soils in the Australia-Pacific Region: state of knowledge and research priorities.
971 *Australian Journal of Botany* 63(4):173–190
972
973 van der Ent A, Mulligan DM (2015) Multi-element concentrations in plants parts and fluids
974 of Malaysian nickel hyperaccumulator plants and some economic and ecological
975 considerations. *Journal of Chemical Ecology* 41:396–408.
976
977 van der Ent A, Callahan DL, Noller BN, Mesjasz-Przybyłowicz J, Przybyłowicz WJ,
978 Barnabas A, Harris HH (2017a) Nickel biopathways in tropical nickel
979 hyperaccumulating trees from Sabah (Malaysia). *Scientific Reports* 7:41861.
980
981 van der Ent A, Przybyłowicz WJ, de Jonge MD, Harris HH, Ryan CG, Tylko G, Paterson DJ,
982 Barnabas AD, Kopittke PM, Mesjasz-Przybyłowicz J (2017b) X-ray elemental
983 mapping techniques for elucidating the ecophysiology of hyperaccumulator plants.
984 *New Phytologist* 218:432–452.
985 van der Ent A, Cardace D, Tibbett M, Echevarria G (2018a) Ecological implications of
986 pedogenesis and geochemistry of ultramafic soils in Kinabalu Park (Malaysia).
987 *Catena* 160: 154–169.
988
989 van der Ent A, Harris HH, Erskine, PD Echevarria G (2018b) Simultaneous
990 hyperaccumulation of nickel and cobalt in *Glochidion* cf. *sericeum* (Phyllanthaceae):
991 elemental distribution and speciation. *Scientific Reports* 8:9683.
992
993 van der Ent A, Mulligan DR, Repin R, Erskine PD (2018c) Foliar elemental profiles in the
994 ultramafic flora of Kinabalu Park (Sabah, Malaysia). *Ecological Research* 33(3):659–
995 674.
996
997 Wang YD, Mesjasz-Przybyłowicz J, Tylko G, Barnabas AD, Przybyłowicz WJ (2013)
998 Micro-PIXE analyses of frozen-hydrated semi-thick biological sections. *Nuclear*

999	Instruments and Methods in Physics Research Section B: Beam Interactions with
1000	Materials and Atoms 306:134–139.
1001	
1002	

1003 **FIGURE CAPTIONS**

1004

1005 **Figure 1.** *Geissois pruinosa* var. *pruinosa* (Cunoniaceae) cauliflorous inflorescences (a),
1006 *Psychotria gabriellae* (Rubiaceae) branch with leaves and inflorescences (b), *Hybanthus*
1007 *austrocaledonicus* (Violaceae) branch with leaves and inflorescence (c), *Homalium francii*
1008 (Salicaceae) branch with leaves (d), *Pycnandra acuminata* (Sapotaceae) branch with leaves
1009 (e), and cut bark of stem exuding latex (f).\

1010

1011 **Figure 2.** Geographical distribution of *Geissois pruinosa* (all varieties), *Psychotria*
1012 *gabriellae*, *Homalium francii*, *Hybanthus austrocaledonicus* and *Pycnandra acuminata* in
1013 New Caledonia on the basis of herbarium (NOU) records. Map generated by ArcGIS (Esri).

1014

1015 **Figure 3.** Boxplots of the foliar concentrations of K, Mg, Ca and Mn, Co*, Ni in *Geissois*
1016 *pruinosa* var. *pruinosa* (n = 12), *Psychotria gabriellae* (n = 12, *n = 10), *Homalium francii* (n
1017 = 12), *Hybanthus austrocaledonicus* (n = 10; *n = 9) and *Pycnandra acuminata* (n=12).
1018 Boxplots show ranges, medians, percentiles and outliers. All values in $\mu\text{g g}^{-1}$ dry weight.

1019

1020 **Figure 4.** Synchrotron μXRF maps of K and Ca of freeze-dried leaf portions of *Geissois*
1021 *pruinosa* var. *pruinosa*, *Psychotria gabriellae*, *Homalium francii*, *Hybanthus*
1022 *austrocaledonicus* and *Pycnandra acuminata*. The maps measure 21.65×2.65 mm at 11 μm
1023 resolution with 10 ms dwell (*Hybanthus*), 17.85×10.29 mm at 17 μm resolution with 10 ms
1024 dwell (*Homalium*), 23.27×7.39 mm at 10 μm resolution with 8 ms dwell (*Psychotria*), 16.63
1025 $\times 11.91$ mm at 10 μm resolution with 8 ms dwell (*Geissois*), and 17.52×11.91 mm at 10 μm
1026 resolution with 8 ms dwell (*Pycnandra*). Maps were cropped to fit figure panels.

1027

1028 **Figure 5.** Synchrotron μXRF maps of Ni, Co and/or Mn of freeze-dried leaf portions of
1029 *Geissois pruinosa* var. *pruinosa*, *Psychotria gabriellae*, *Homalium francii*, *Hybanthus*
1030 *austrocaledonicus* and *Pycnandra acuminata*. The maps measure 21.65×2.65 mm at 11 μm
1031 resolution with 10 ms dwell (*Hybanthus*), 17.85×10.29 mm at 17 μm resolution with 10 ms
1032 dwell (*Homalium*), 23.27×7.39 mm at 10 μm resolution with 8 ms dwell (*Psychotria*), 16.63
1033 $\times 11.91$ mm at 10 μm resolution with 8 ms dwell (*Geissois*), and 17.52×11.91 mm at 10 μm
1034 resolution with 8 ms dwell (*Pycnandra*). Maps were cropped to fit figure panels.

1035

1036 **Figure 6.** Synchrotron μ XRF maps of K, Ca, Ni and Mn of fresh leaf portions of *Geissois*
1037 *pruinosa* var. *pruinosa*, and *Psychotria gabriellae*. The maps measure 29.39×9.15 mm at 8
1038 μ m resolution with 17 ms dwell (*Geissois*) and 16.2×12.3 mm at 15 μ m resolution with 10
1039 ms dwell (*Psychotria*). Maps were cropped to fit figure panels.

1040

1041 **Figure 7.** Synchrotron μ XRF maps of K, Ca, Ni and Mn of fresh leaf midrib portions of
1042 *Psychotria gabriellae* and *Pycnandra acuminata*. The maps measure 3.49×2.12 mm at 8 μ m
1043 resolution with 10 ms dwell (*Psychotria*) and 7.4×2.8 mm at 6 μ m resolution with 8 ms
1044 dwell (*Pycnandra*). Maps were cropped to fit figure panels.

1045

1046 **Figure 8.** Synchrotron μ XRF maps of K and Ca of freeze-dried petiole portions of *Homalium*
1047 *francii*; and of fresh petioles portions of *Psychotria gabriellae*, *Geissois pruinosa* var.
1048 *pruinosa* and *Pycnandra acuminata*. The maps measure 2.28×4.49 mm at 5 μ m resolution
1049 with 10 ms dwell (*Homalium*), 5.5×3.08 mm at 8 μ m resolution with 8 ms dwell
1050 (*Psychotria*), 6.3×5.68 mm at 7 μ m resolution with 8 ms dwell (*Geissois*), and 3.9×2.35
1051 mm at 5 μ m resolution with 8 ms dwell (*Pycnandra*). Maps were cropped to fit figure panels.

1052

1053 **Figure 9.** Synchrotron μ XRF maps of Ni and Zn, of freeze-dried petiole portions of
1054 *Homalium francii*; and Ni and Mn or Co of fresh petioles portions of *Psychotria gabriellae*,
1055 *Geissois pruinosa* var. *pruinosa* and *Pycnandra acuminata*. The maps measure 2.28×4.485
1056 mm at 5 μ m resolution with 10 ms dwell (*Homalium*), 5.5×3.08 mm at 8 μ m resolution with
1057 8 ms dwell (*Psychotria*), 6.3×5.68 mm at 7 μ m resolution with 8 ms dwell (*Geissois*), and
1058 3.9×2.35 mm at 5 μ m resolution with 8 ms dwell (*Pycnandra*). Maps were cropped to fit
1059 figure panels.

1060

1061 **Figure 10.** Synchrotron μ XRF maps of K, Ca, Ni and Zn, of fresh stem portions of
1062 *Psychotria gabriellae*. The maps measure 4.7×4.58 mm at 8 μ m resolution with 8 ms dwell.
1063 Maps were cropped to fit figure panels.

1064

1065 **Figure 11.** Synchrotron μ XRF maps of K, Ca, Mn, Co, Ni and Zn, of fresh leaf blade cross
1066 section of *Psychotria gabriellae*. The maps measure 0.16×0.27 mm at 0.5 μ m resolution
1067 with 15 ms dwell (*Psychotria*). Maps were cropped to fit figure panels.

1068

Table 1. Habitat soil elemental concentrations in the natural habitats of *Geissois pruinosa* var. *pruinosa*, *Hybanthus austrocaledonicus*, *Psychotria gabriellae* and *Pycnandra acuminata*. The concentration values are ranges and means in $\mu\text{g g}^{-1}$ or in mg g^{-1} when indicated with an asterisk* expressed on dry weight basis. The digests and extracts were analysed with ICP-AES. The ‘total’ is extractable with HCL/HNO₃ digest, ‘DTPA’ is extractable with Diethylenetriamine pentaacetic acid solution, and ‘Sr(NO₃)₂’ is extractable with strontium nitrate solution. The *Homalium francii* samples were collected in close proximity of *Pycnandra acuminata*, therefore the soil habitat chemistry will be similar.

Species	n	Habitat soil chemistry					
		pH	Mg (total)*	Al (total)*	P (total)	S (total)	K (total)
<i>Geissois pruinosa</i> var. <i>pruinosa</i>	3	6.1–6.2 [6.2]	15.2–20.1 [18.4]	12.2–14.6 [13.2]	278–305 [296]	585–959 [712]	233 ^a
<i>Hybanthus austrocaledonicus</i>	1	5.9	7.2	34.9	295	648	—
<i>Psychotria gabriellae</i>	3	5.1–5.9 [5.4]	8.8–14.1 [11.9]	22.3–31.9 [28.1]	751–779 [765]	887–1200 [1080]	231–864 [627]
<i>Pycnandra acuminata</i>	1	5.8	5.2	42.5	373	716	224
Species	n	Ca (total)	Cr (total)*	Cr (DTPA)	Cr (Sr(NO ₃) ₂)	Mn (total)	Mn (DTPA)
<i>Geissois pruinosa</i> var. <i>pruinosa</i>	3	1270–1550 [1370]	6.7–8.0 [7.3]	0.3–0.5 [0.4]	0.1–0.3 [0.2]	4160–4320 [4230]	571–614 [594]
<i>Hybanthus austrocaledonicus</i>	1	1020	6.6	0.2	0.2	7080	842
<i>Psychotria gabriellae</i>	3	1370–3250 [2510]	1.8–12 [5.4]	0.5–1 [0.9]	0.2–0.7 [0.6]	2880–4670 [3540]	780–1090 [891]
<i>Pycnandra acuminata</i>	1	459	8.6	0.5	0.1	7280	875
Species	n	Mn (Sr(NO ₃) ₂)	Fe (total)*	Fe (Sr(NO ₃) ₂)	Co (total)	Co (DTPA)	Co (Sr(NO ₃) ₂)
<i>Geissois pruinosa</i> var. <i>pruinosa</i>	3	16.1–20.5 [18.1]	354–388 [366]	0.04–0.3 [0.2]	845–933 [875]	55.6–58.7 [57.1]	0.7–0.9 [0.8]
<i>Hybanthus austrocaledonicus</i>	1	30.6	289	0.1	952	48.6	0.4
<i>Psychotria gabriellae</i>	3	32.9–285 [181]	128–375 [217]	0.1–16 [9.7]	339–638 [445]	71.3–77.8 [75.4]	0.7–8 [5]
<i>Pycnandra acuminata</i>	1	105	346	0.2	1080	65.5	1.3
Species	n	Ni (total)*	Ni (DTPA)	Ni (Sr(NO ₃) ₂)	Zn (total)	Zn (DTPA)	Zn (Sr(NO ₃) ₂)
<i>Geissois pruinosa</i> var. <i>pruinosa</i>	3	9.9–10.5 [10.2]	320–426 [367]	6.4–8.2 [7.1]	324–345 [336]	13.1–15.5 [13.9]	0.3–0.4 [0.3]
<i>Hybanthus austrocaledonicus</i>	1	8	627	18.2	287	10.5	0.3

<i>Psychotria gabriellae</i>	3	2.7–5.7 [3.7]	300–443 [352]	8.4–26.3 [18.9]	204–322 [250]	7.5–67.5 [46.1]	0.4–4.1 [2.8]
<i>Pycnandra acuminata</i>	1	8.3	599	38	321	9.8	0.9

^a Only one sample, * ranges and means in mg g⁻¹, n = number of analysed samples

Table 2. Bulk macro-elemental concentrations of various plant parts of *Geissois pruinosa* var. *pruinosa*, *Homalium francii*, *Hybanthus austrocaledonicus*, *Psychotria gabriellae*, and *Pycnandra acuminata*. The concentration values are ranges and means in $\mu\text{g g}^{-1}$ or in mg g^{-1} when indicated with an asterisk* expressed on dry weight basis. Hash# indicates sample size if different from the n. Acid digests and were analysed with ICP-AES.

Species	n	Ca	Fe	K	Mg	Na	P	S
Leaves								
<i>Geissois pruinosa</i> var. <i>pruinosa</i>	12	2.97–4.7 [3.91]	10–46 [29]	1.09–1.83 [1.35]	1.83–5.17 [4.16]	220–740 [400]	92–490 [270]; 11#	0.51–8.32 [1.87]
<i>Homalium francii</i>	12	1.24–3.61 [2.02]	37–300 [140]	1.17–10.4 [5.84]	1.2–3.33 [2.27]	130–3090 [1810]	160–1460 [580]	0.85–3.48 [2.02]
<i>Hybanthus austrocaledonicus</i>	10	1.16–2.29 [1.71]	31–71 [47]	1.83–10.200 [6.28]	2.76–4.9 [3.4]	730–6000 [2400]	7–680 [360]; 8#	1.14–3.82 [2.75]
<i>Psychotria gabriellae</i>	12	1.40–5.17 [2.82]	19–1510 [170]	0.48–19.0 [3.09]	0.91–2.93 [1.6]	390–2180 [950]	140–860 [480]; 10#	0.75–5.27 [2.94]
<i>Pycnandra acuminata</i>	12	0.66–5.62 [1.23]	26–340 [81]	3.3–7.74 [5.20]	0.51–1.85 [0.98]	1130–2590 [1580]	55–810 [290]	0.51–1.93 [1.17]
Branches								
<i>Geissois pruinosa</i> var. <i>pruinosa</i>	3	0.84–5.26 [3.47]	7.7–12 [9.2]	0.44–1.89 [1.05]	0.51–1.8 [1.04]	140–330 [230]	110–600 [330]	0.33–0.75 [0.480]
<i>Homalium francii</i>	3	3.67–5.46 [4.36]	63–76 [71]	1.3–2.56 [1.74]	0.55–1.13 [0.91]	160–190 [170]	87–220 [140]	0.36–0.71 [0.52]
<i>Hybanthus austrocaledonicus</i>	2	1.66–1.700 [1.68]	7–15 [11]	2.19–2.97 [2.58]	0.44–0.8 [0.62]	610–670 [640]	130–170 [150]	0.47–0.73 [0.6]
<i>Psychotria gabriellae</i>	4	2.26–4.68 [3.01]	15–45 [26]	2.65–4.47 [3.39]	0.23–0.61 [0.35]	270–2710 [1150]	69–160 [110]	0.52–0.7 [0.59]
<i>Pycnandra acuminata</i>	2	1.55–4.26 [2.90]	180–1030 [610]	1.77–4.38 [3.07]	0.43–2.44 [1.44]	1600–1850 [1720]	340–740 [540]	0.72–1.04 [0.88]
Bark								
<i>Geissois pruinosa</i> var. <i>pruinosa</i>	1	16.3	9.1	0.61	2.11	75	100	0.81
<i>Homalium francii</i>	1	24.8	15	2.56	0.24	37	170	0.74
<i>Hybanthus austrocaledonicus</i>	4	0.93–1.44 [1.17]	15–240 [82]	7.69–8.88 [8.38]	0.37–0.74 [0.52]	21–350 [150]	93–220 [170]	0.76–2.47 [1.38]
<i>Pycnandra acuminata</i>	2	0.6–5.28 [2.94]	21–22 [22]	0.43–0.49 [0.46]	0.07–0.0199 [0.09]	840–3780 [2310]	51–82 [66]	0.3–1.0 [0.65]
Roots								
<i>Homalium francii</i>	1	2.13	5710	1950	1.92	1920	240	0.71
<i>Hybanthus austrocaledonicus</i>	2	0.77–5.13 [2.95]	870–1620 [1250]	2.41–2.46 [2.44]	0.53–1.73 [1.13]	53–390 [220]	140–220 [180]	0.74–0.97 [0.85]
<i>Psychotria gabriellae</i>	2	0.26–6.43 [3.35]	1080–2870 [1970]	1.51–1.73 [1.62]	0.34–1.17 [0.75]	930–1430 [1180]	160–2310 [1240]	0.76–0.81 [0.79]
Flowers								
<i>Geissois pruinosa</i> var. <i>pruinosa</i>	2	3.56–5.18 [4.37]	15–15 [15]	5.09–7.35 [6.22]	2.58–3.43 [3.0]	210–1040 [620]	530–860 [700]	1.14–1.75 [1.44]
<i>Psychotria gabriellae</i>	2	3.76–3.88 [3.82]	28–38 [33]	9.57–9.58 [9.57]	1.94–2.48 [2.21]	180–640 [410]	740–760 [750]	0.59–2.04 [1.31]
Fruits (pericarp except for <i>P. gabriellae</i>)								
<i>Geissois pruinosa</i> var. <i>pruinosa</i>	1	2.47	11	4.14	1.64	940	730	0.87
<i>Psychotria gabriellae</i>	3	2.05–5.92 [3.94]	12–17 [15]	7.15–8.5 [7.82]	1.9–2.15 [2.03]	240–390 [310]	610–950 [760]	1.47–1.66 [1.59]
<i>Pycnandra acuminata</i>	2	0.91–2.48 [1.7]	14–20 [17]	4.39–4.81 [4.600]	0.63–2.18 [1.41]	680–1180 [930]	200–680 [440]	0.67–0.91 [0.79]
Seeds (with endocarp in <i>P. gabriellae</i>)								

<i>Psychotria gabriellae</i>	1	2.1	13	2.44	1.5	54	1000	1.39
<i>Pycnandra acuminata</i>	1	0.78	9.8	2.69	0.74	830	560	0.43
Latex								
<i>Pycnandra acuminata</i>	2	7.46–17.04 [12.25]	61–200 [130]	1.14–3.8 [2.47]	0.48–1.36 [0.92]	1560–3320 [2440]	310–570 [440]	0.7–1.19 [0.94]

Table 3. Bulk trace elemental concentrations of various plant parts of *Geissois pruinosa* var. *pruinosa*, *Homalium francii*, *Hybanthus austrocaledonicus*, *Psychotria gabriellae*, and *Pycnandra acuminata*. The concentration values are ranges and means in $\mu\text{g g}^{-1}$ or in mg g^{-1} when indicated with an asterisk* expressed on dry weight basis. Hash# indicates sample size if different from the n. Acid digests and were analysed with ICP-AES.

Species	n	Al	Co	Cr	Cu	Mn	Ni	Zn
Leaves								
<i>Geissois pruinosa</i> var. <i>pruinosa</i>	12	9.3–62 [42]	0.5–55 [39]	3.4–78 [56]	1.9–7.4 [2.3]	56–180 [93]	3.21–10.6 [8.99]	25–57 [39]
<i>Homalium francii</i>	12	11–230 [100]	0.1–120 [28]	4–120 [39]	5.1–29 [12]	24–76 [45]	2.65–9.48 [5.4]	26–220 [110]
<i>Hybanthus austrocaledonicus</i>	10	57–97 [75]	1.8–130 [30]; 9#	5.9–81 [38]; 7#	1.3–9.8 [6.6]	77–180 [120]	9.22–15.6 [12.7]	48–260 [100]
<i>Psychotria gabriellae</i>	12	20–160 [90]	3.2–90 [37]; 10#	1.2–51 [27]; 9#	3–36 [12]; 11#	22–140 [72]	10.2–32.200 [21.4]	14–200 [95]
<i>Pycnandra acuminata</i>	12	16–170 [69]	0.3–73 [18]	2.2–41 [19]; 9#	0.1–9.7 [2.4]	21–51 [28]	6.71–17.9 [13.3]	23–94 [50]
Branches								
<i>Geissois pruinosa</i> var. <i>pruinosa</i>	3	5.6–7.7 [6.5]	2.3–12 [5.7]	0.7–1.8 [1.3]	3.1–21 [9.9]	9.7–22 [15]	0.47–1.07 [0.72]	24–56 [39]
<i>Homalium francii</i>	3	16–19 [18]	0.2–1.7 [0.9]	2.7–2.9 [1.2]	1–8.4 [1.4]	8.8–17 [14]	0.87–0.95 [0.92]	20–25 [22]
<i>Hybanthus austrocaledonicus</i>	2	4.9–6.1 [2.3]	0.1–0.9 [0.5]	0.5–1.7 [1.1]	1.3–1.6 [1.5]	21–25 [23]	2.03–2.34 [2.18]	13–14 [14]
<i>Psychotria gabriellae</i>	4	6–22 [12]	0.5–2.8 [2]	1.1–3.3 [2]	2.6–4.7 [3.9]	14–73 [35]	4.61–14.6 [8.12]	22–53 [33]
<i>Pycnandra acuminata</i>	2	29–130 [82]	0.3–0.4 [0.3]	0.9–31 [16]	3.2–9.4 [6.3]	23–64 [44]	2.82–6.86 [4.84]	25–32 [28]
Bark								
<i>Geissois pruinosa</i> var. <i>pruinosa</i>	1	11	6.3	1.3	2.6	25	0.41	24
<i>Homalium francii</i>	1	21	2	0.6	0.5	20	0.92	45
<i>Hybanthus austrocaledonicus</i>	4	8.8–17 [13]	0.5–6.2 [3.3]	5.7–69 [30]	0.3–3 [1.5]	55–170 [130]	7.59–48.5 [26 400]	39–170 [97]
<i>Pycnandra acuminata</i>	2	7.9–13 [10]	0.03–0.3 [0.2]	1.4–2.7 [1.3]	1.8–2.3 [2.1]	5.2–65 [35]	7.99–10.6 [9290]	35–50 [42]
Roots								
<i>Homalium francii</i>	1	740	0.2	140	9.1	110	1.24	36
<i>Hybanthus austrocaledonicus</i>	2	68–250 [160]	0.04–2.2 [1.1]	16–43 [30]	1.6–1.9 [1.7]	120–130 [120]	2.42–3.41 [2.91]	19–22 [21]
<i>Psychotria gabriellae</i>	2	120–160 [140]	0.6–3 [1.8]	25–35 [30]	4–7.2 [5.6]	58–170 [120]	2.2–2.83 [2.51]	14–16 [15]
Flowers								
<i>Geissois pruinosa</i> var. <i>pruinosa</i>	2	7–9.2 [8.1]	7–16 [12]	2.1–3.9 [1.3]	11–17 [14]	28–65 [47]	2.71–3.4 [3.06]	18–32 [25]
<i>Psychotria gabriellae</i>	2	27–60 [44]	0.4–11 [5.8]	0.1–16 [8.1]	4.6–6.3 [5.5]	34–150 [91]	14.51–18.0 [16.3]	43–61 [52]
Fruits (pericarp except for <i>P. gabriellae</i>)								
<i>Geissois pruinosa</i> var. <i>pruinosa</i>	1	5.4	5.2	1.9	11	24	1.51	12
<i>Psychotria gabriellae</i>	3	6.7–19 [12]	0.9–1.6 [1.1]	1.5–7.6 [2.2]	5.2–6 [5.6]	20–25 [22]	8.66–11.3 [9.81]	29–34 [31]
<i>Pycnandra acuminata</i>	2	5.5–6.8 [6.2]	0.03–1 [0.5]	0.4–1.8 [1.1]	3.6–5.8 [2.6]	10–30 [20]	3.68–8.59 [6.13]	13–35 [24]
Seeds (with endocarp in <i>P. gabriellae</i>)								
<i>Psychotria gabriellae</i>	1	7.2	0.2	1.4	6.1	54	5.42	20
<i>Pycnandra acuminata</i>	1	7.1	—	4.7	1.3	22	4.11	14

Latex								
<i>Pycnandra acuminata</i>	2	120–1500 [810]	24–59 [41]	1.9–6.7 [4.3]	2.9–49 [26]	220–340 [280]	110.–154. [132.]	670–920 [800]

figure 1

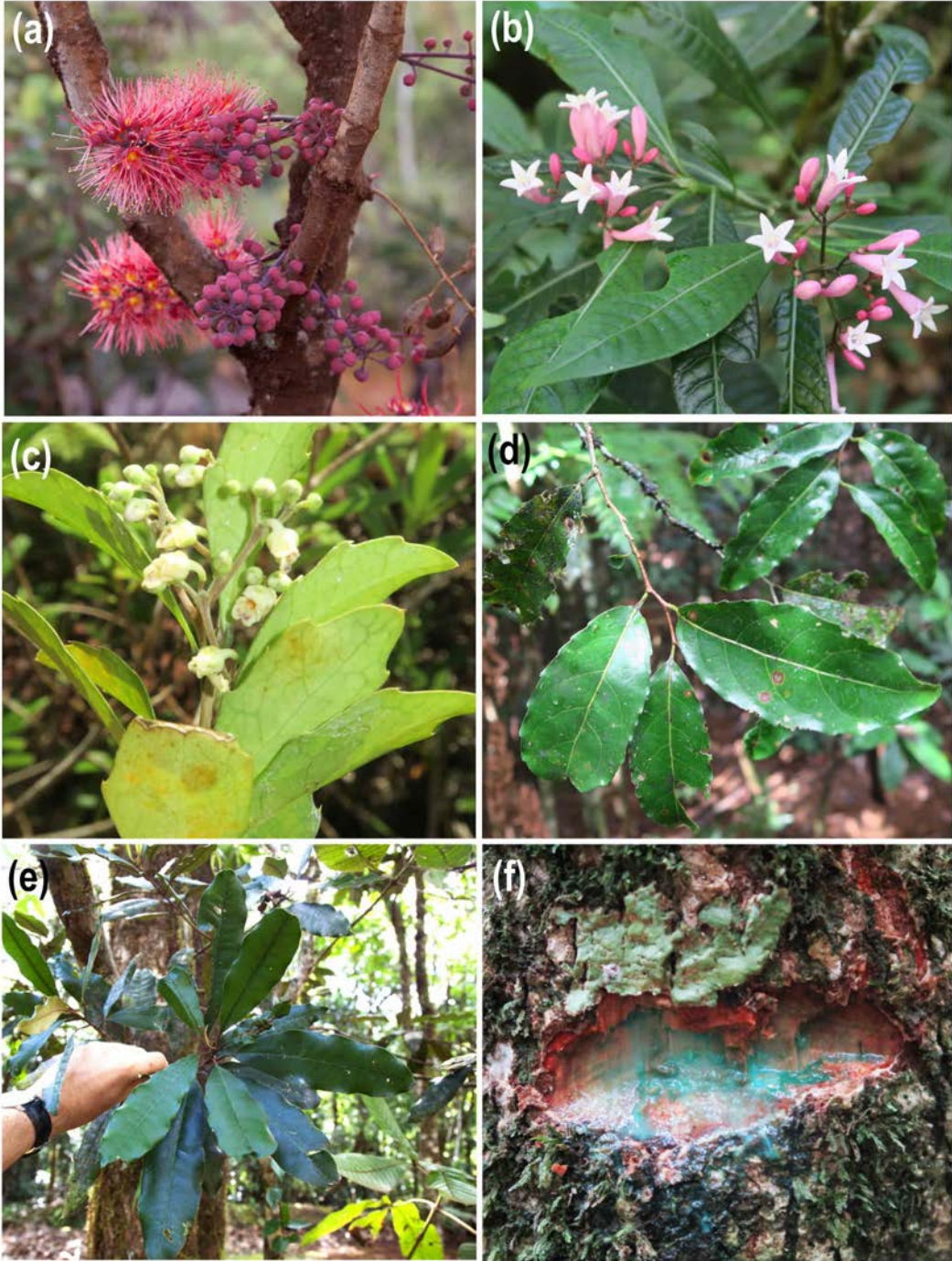


figure 2

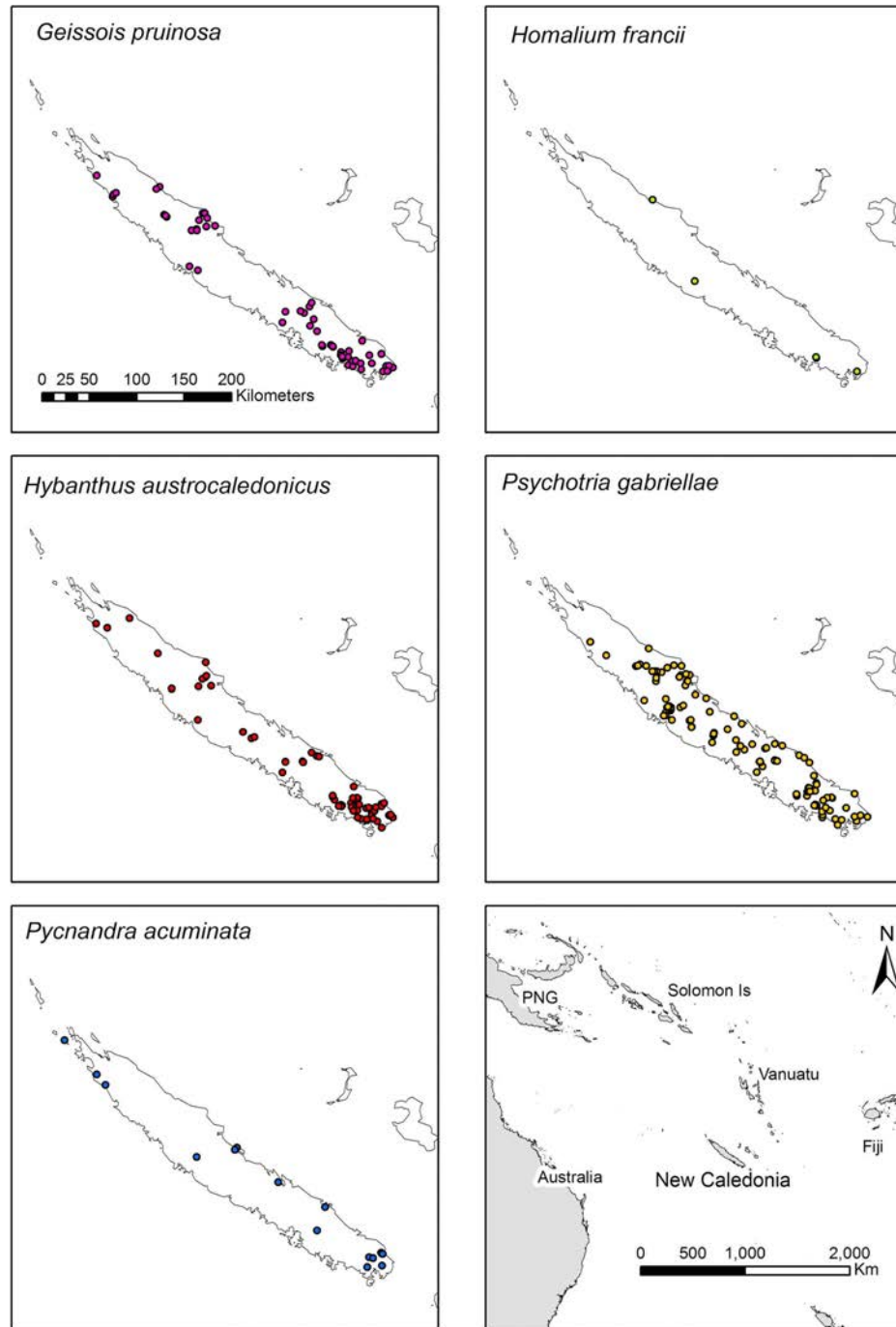


figure 3

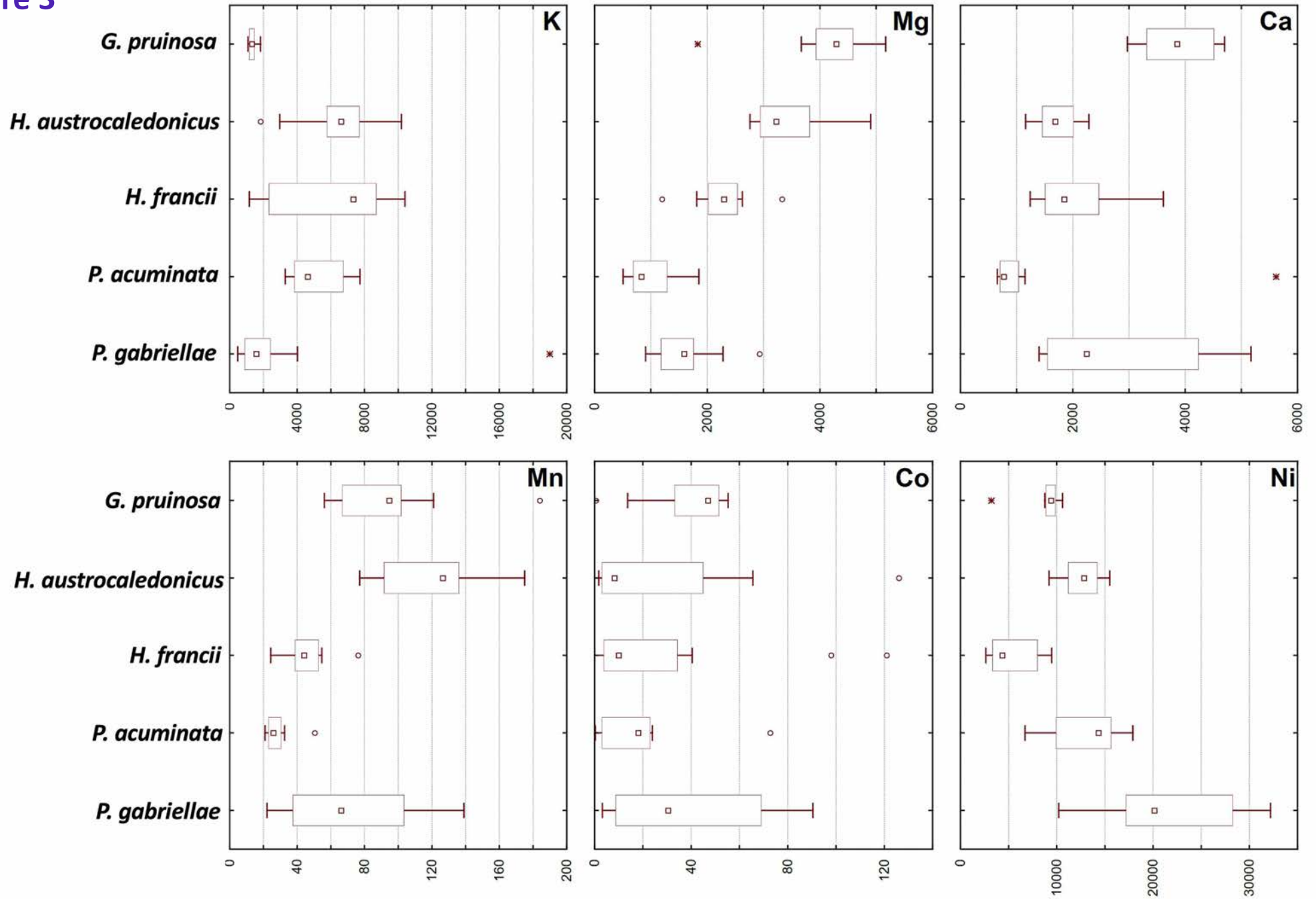


figure 4

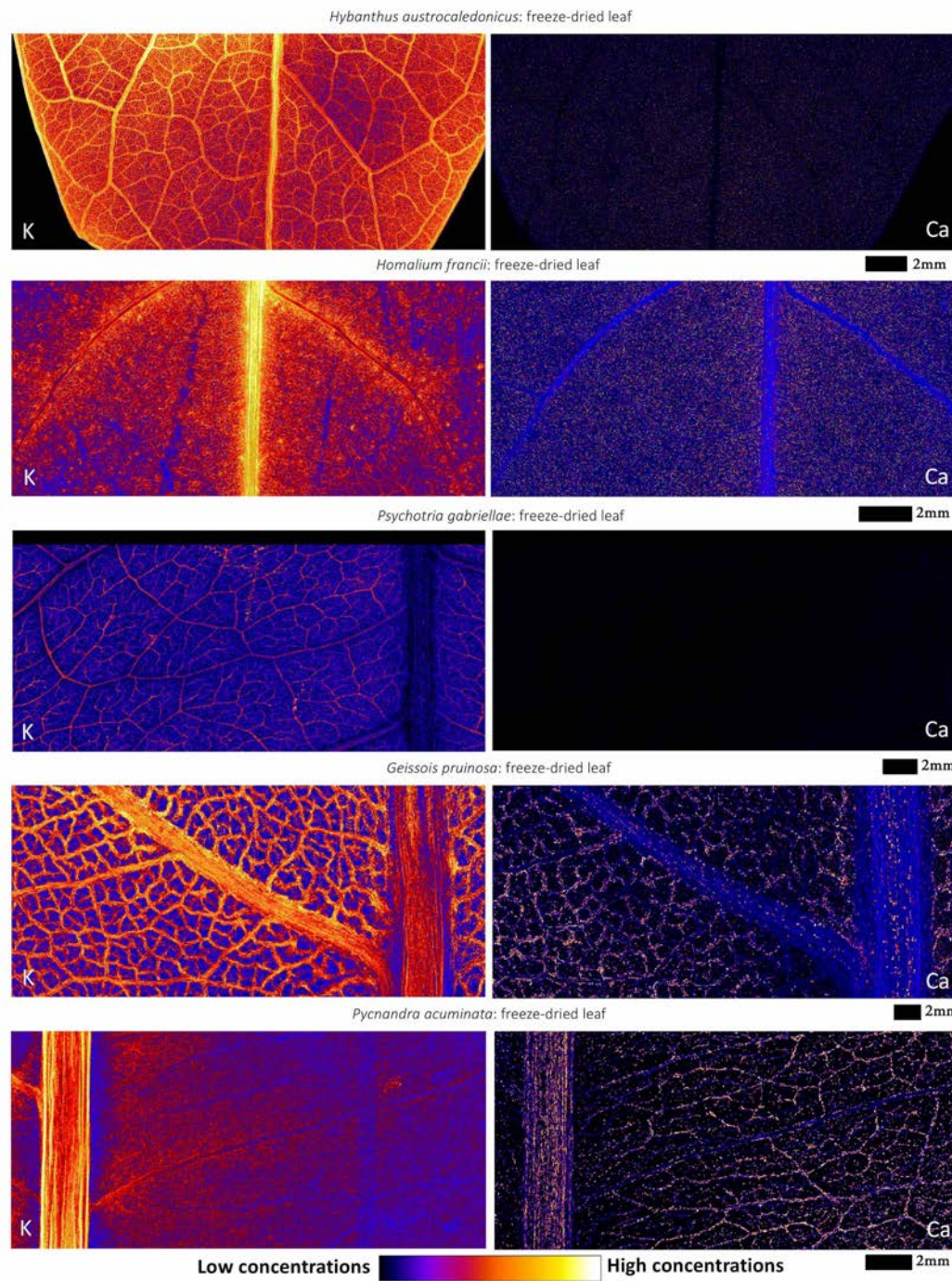


figure 5

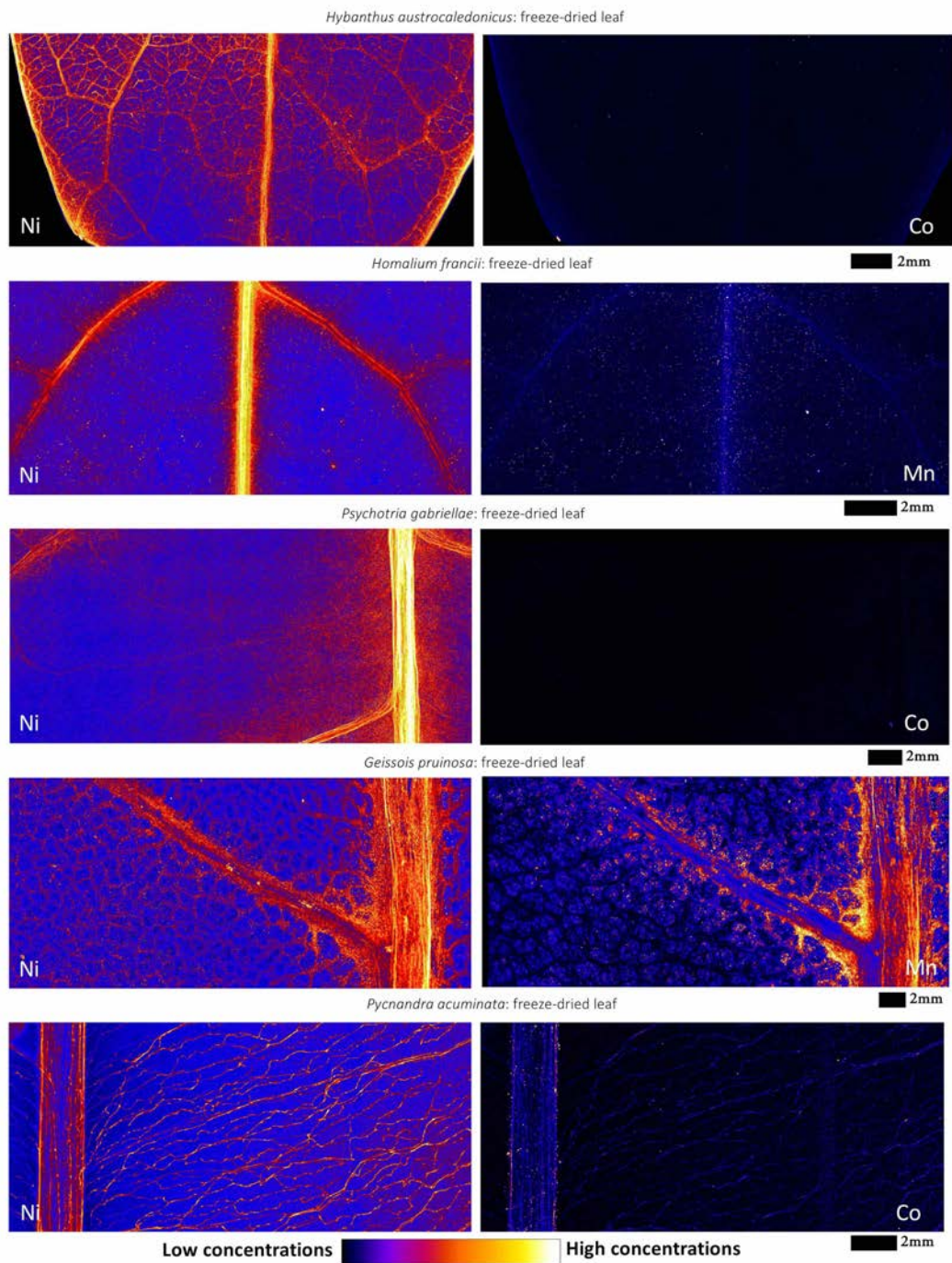


figure 6

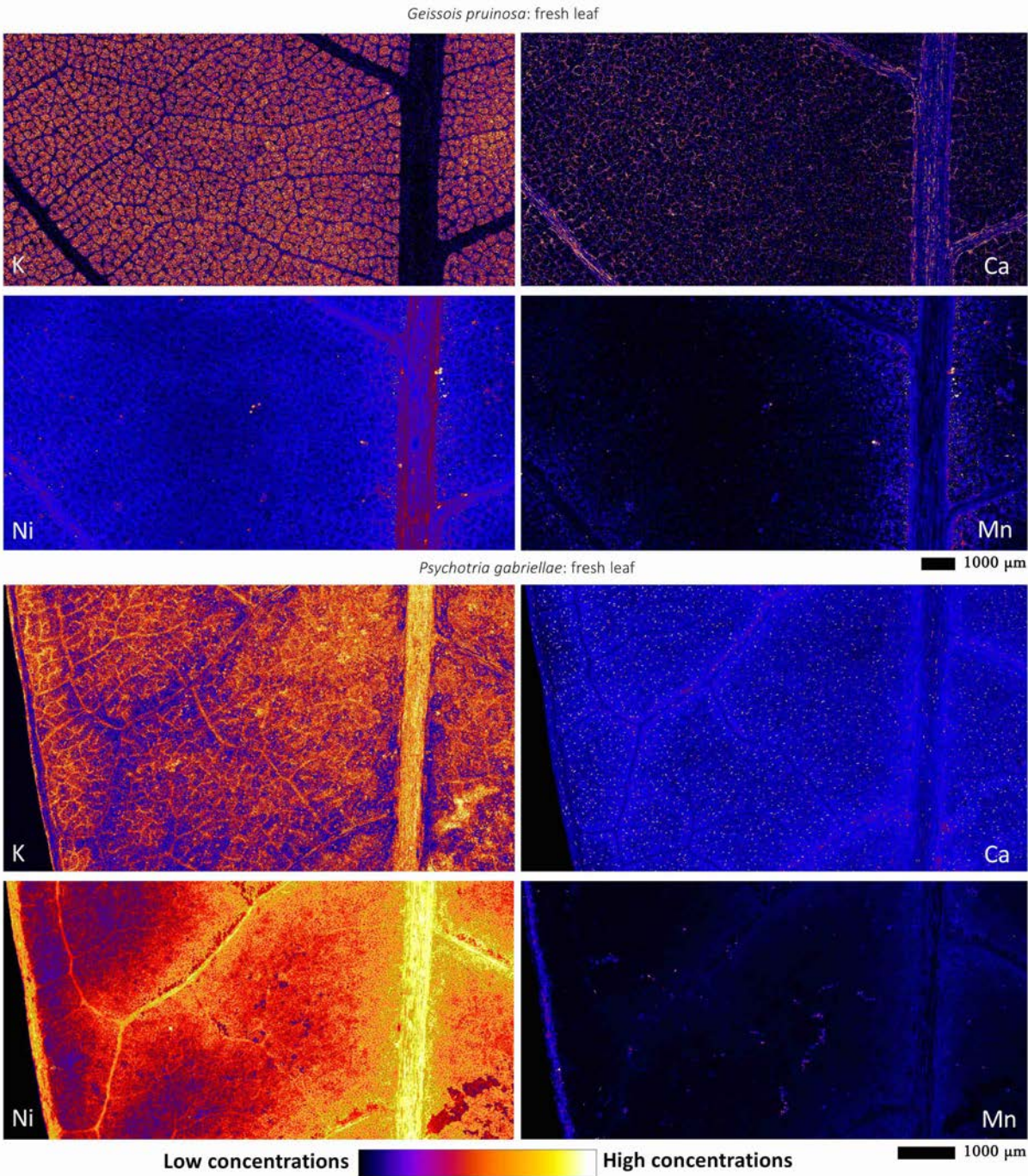


figure 7

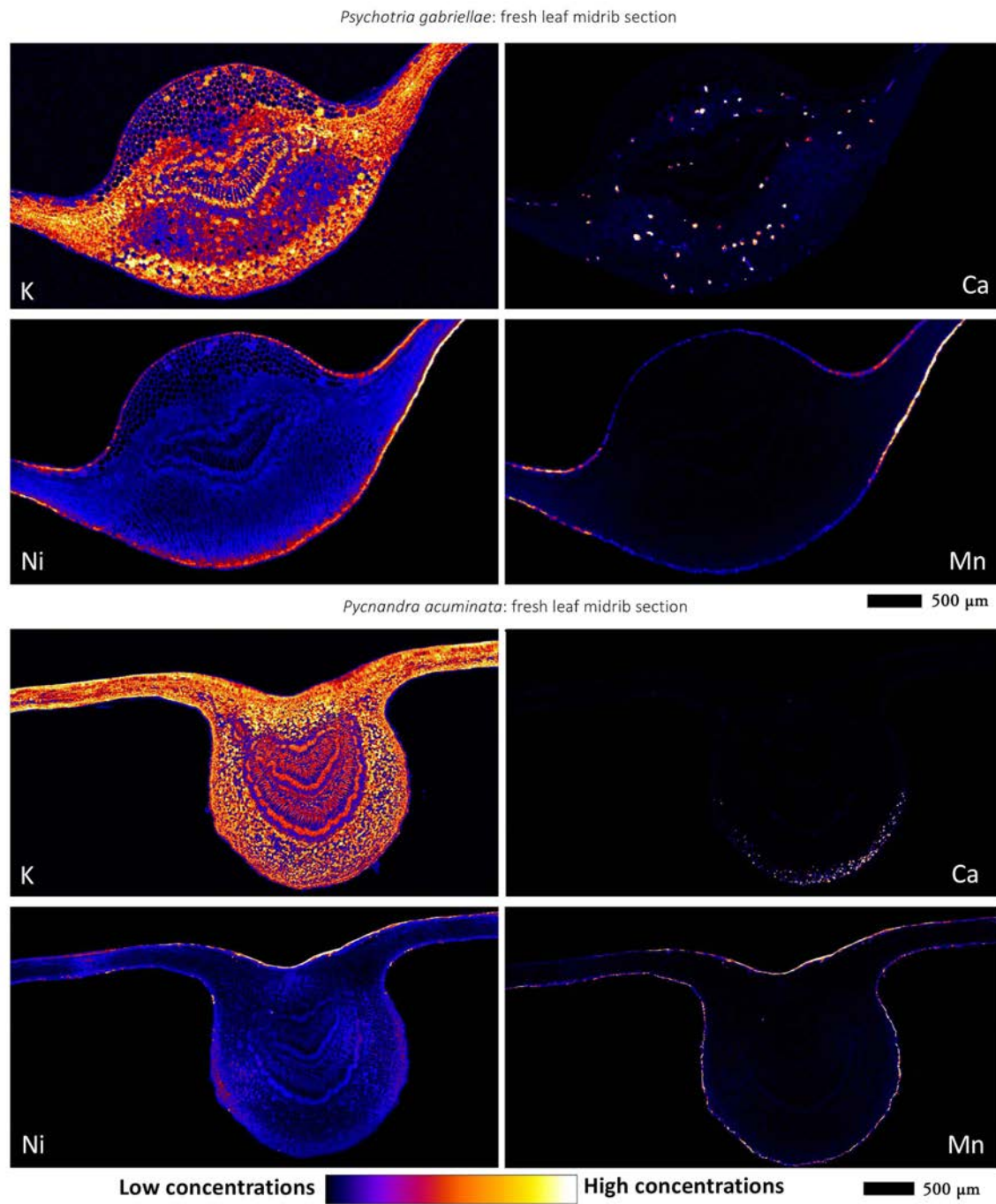


figure 8

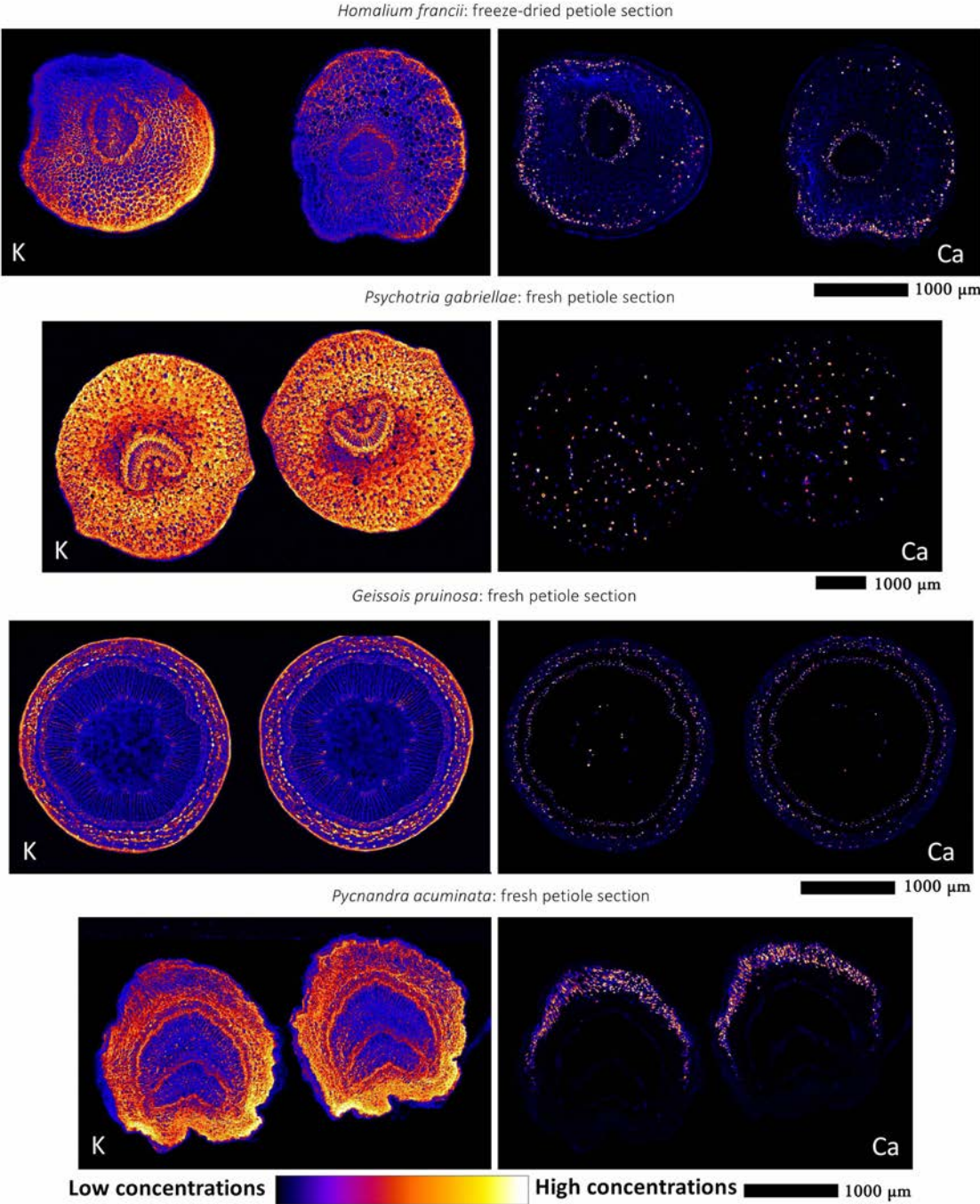


figure 9

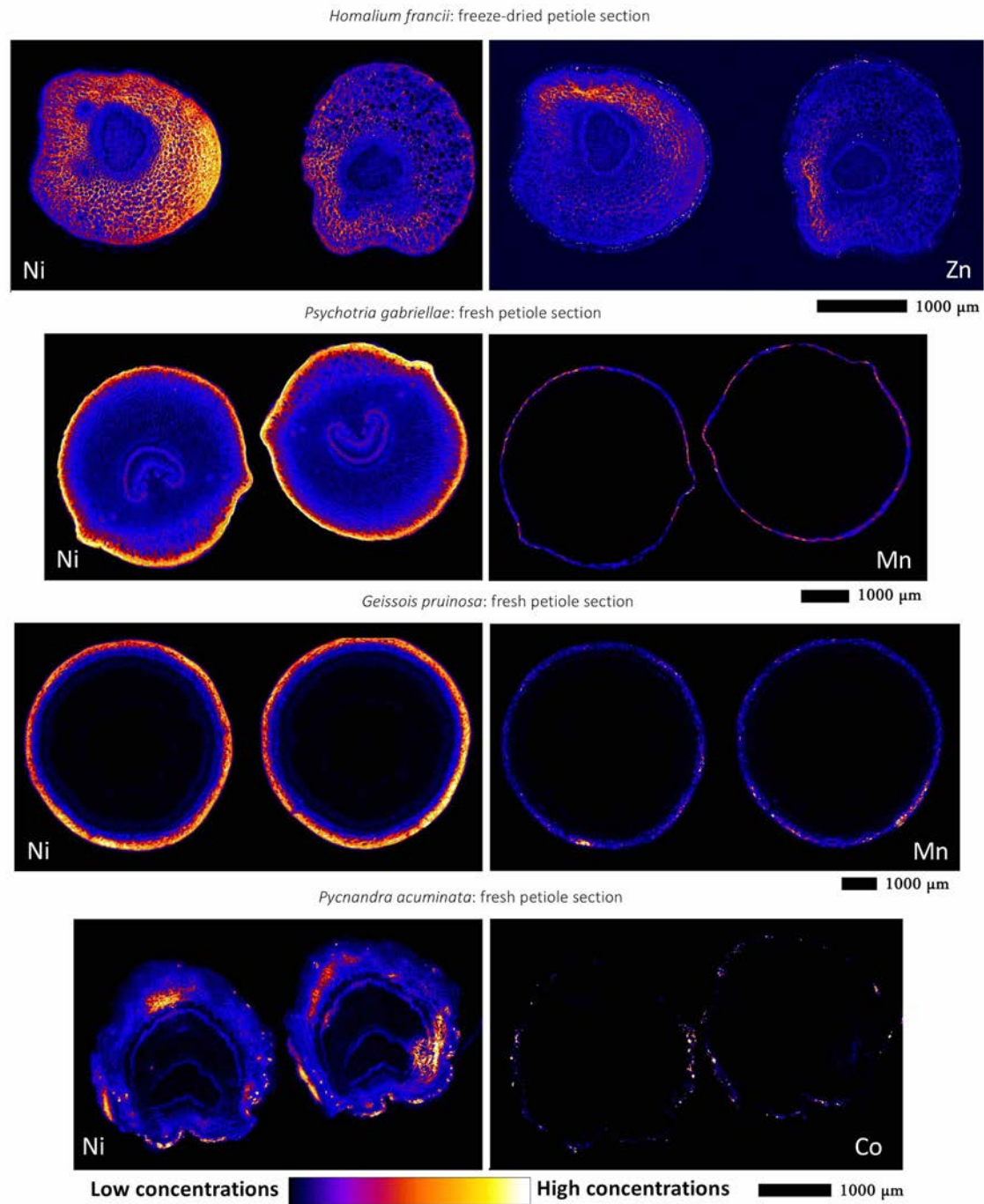


figure 10

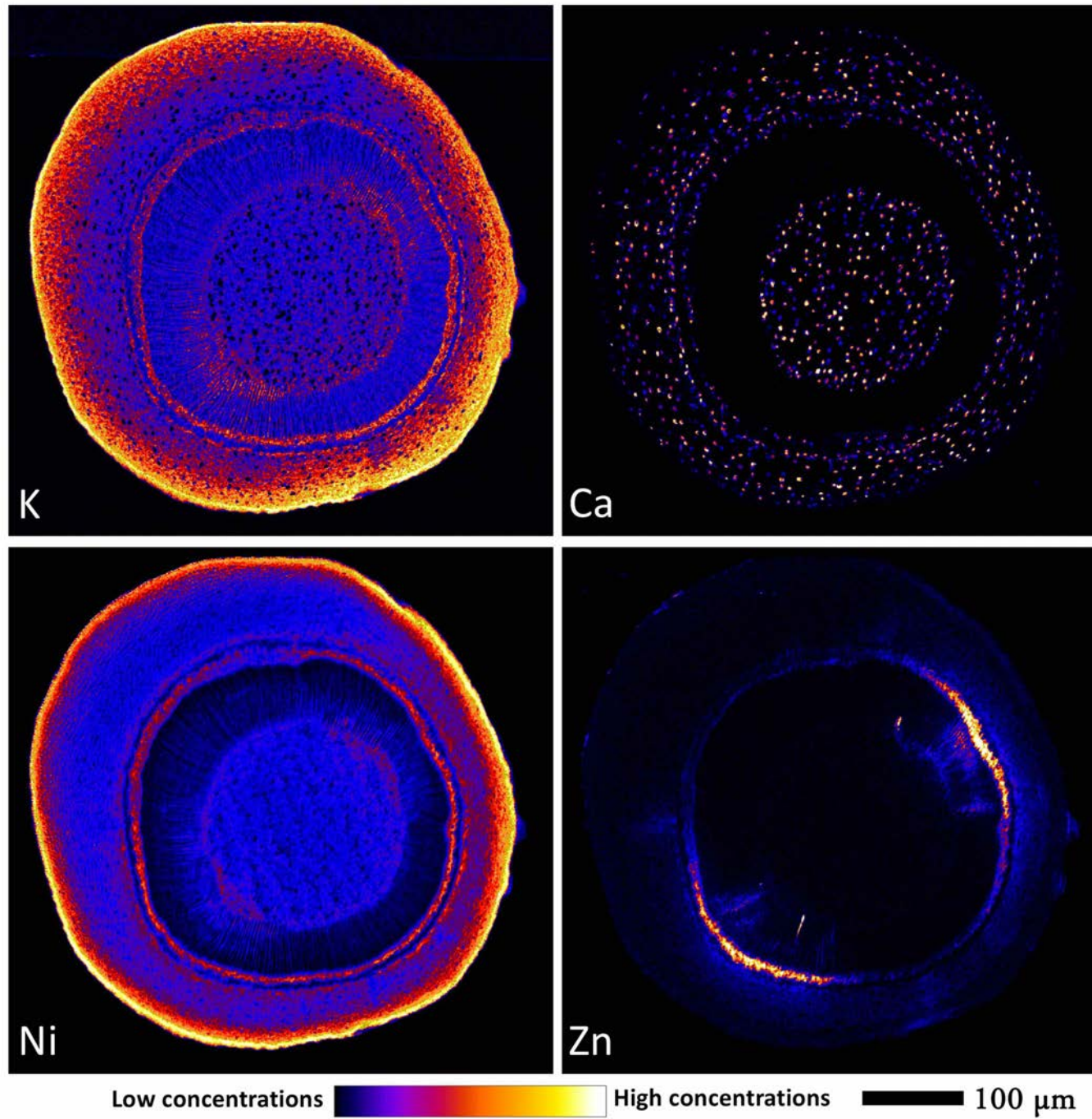
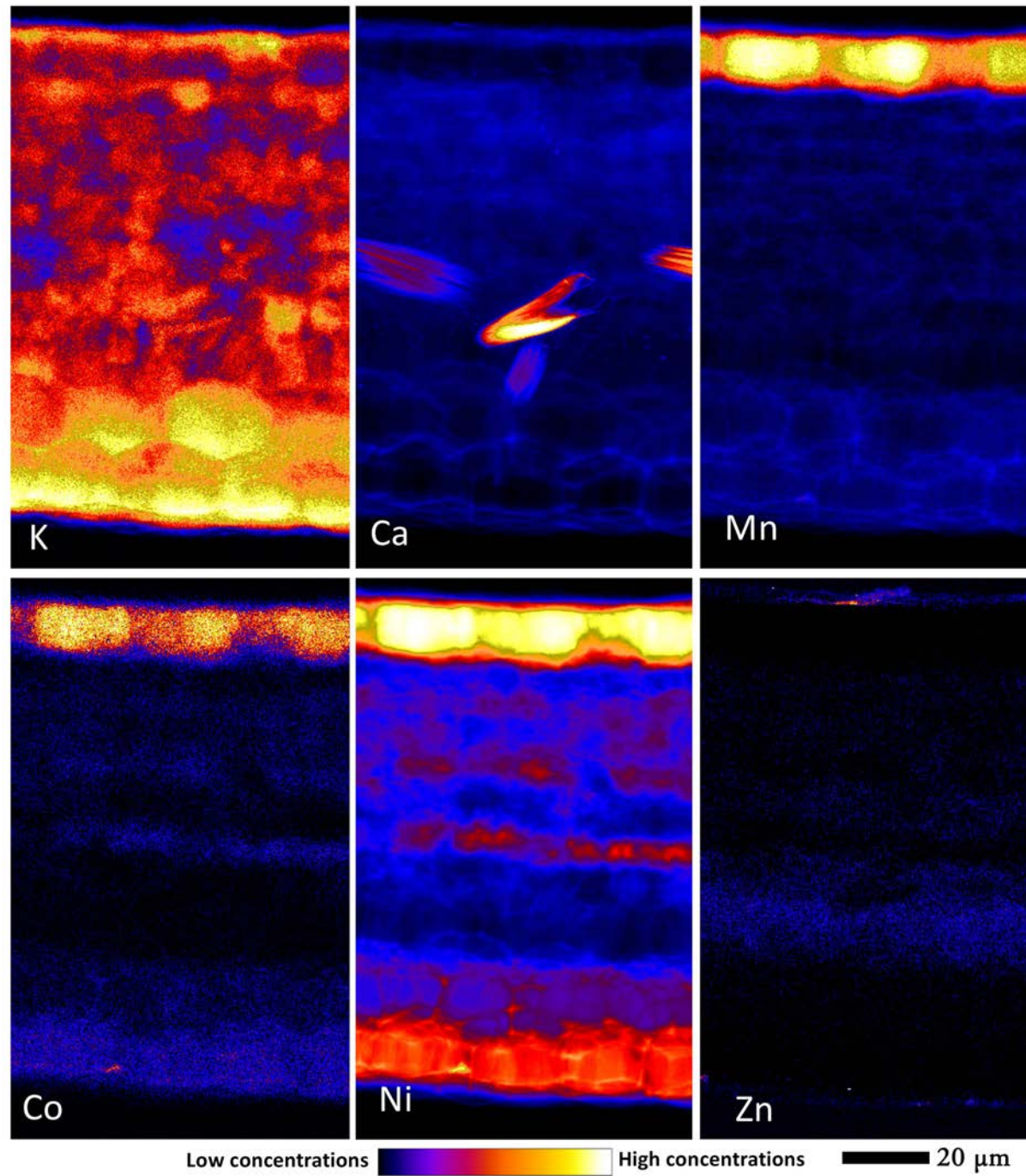


figure 11



SUPPLEMENTARY INFORMATION

Soil chemistry, elemental profiles and elemental distribution in nickel hyperaccumulator species from New Caledonia

Vidiro Gei¹, Guillaume Echevarria^{1,2}, Peter D. Erskine¹, Sandrine Isnard^{3,4}, Bruno Fogliani⁵,
Emmanuelle Montargès-Pelletier⁶, Tanguy Jaffré^{3,4}, Kathryn Spiers⁷,
Jan Garrevoet⁷, Antony van der Ent^{1,2*}

¹Centre for Mined Land Rehabilitation, Sustainable Minerals Institute,
The University of Queensland, Australia.

²Université de Lorraine – INRAE, Laboratoire Sols et Environnement, UMR 1120, France.

³AMAP, Université de Montpellier, IRD, CIRAD, CNRS, INRAE, Montpellier, France.

⁴AMAP, IRD, Herbier de Nouméa, Nouméa, New Caledonia.

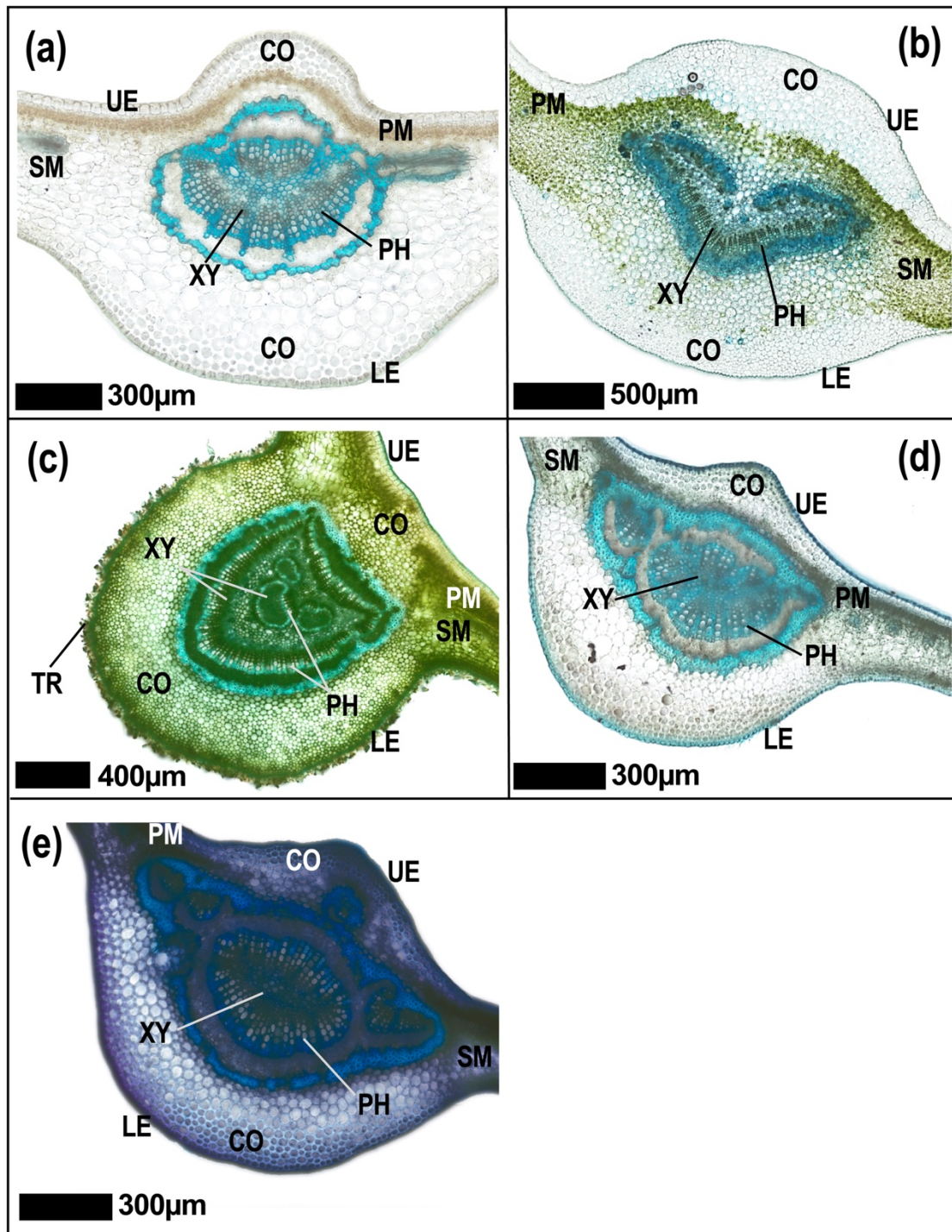
⁵Institut Agronomique néo-Calédonien (IAC), Equipe ARBOREAL (Agriculture
BiODiversité Et vAlorisation), New Caledonia.

⁶Laboratoire Interdisciplinaire des Environnements Continentaux, CNRS,
Université de Lorraine, France.

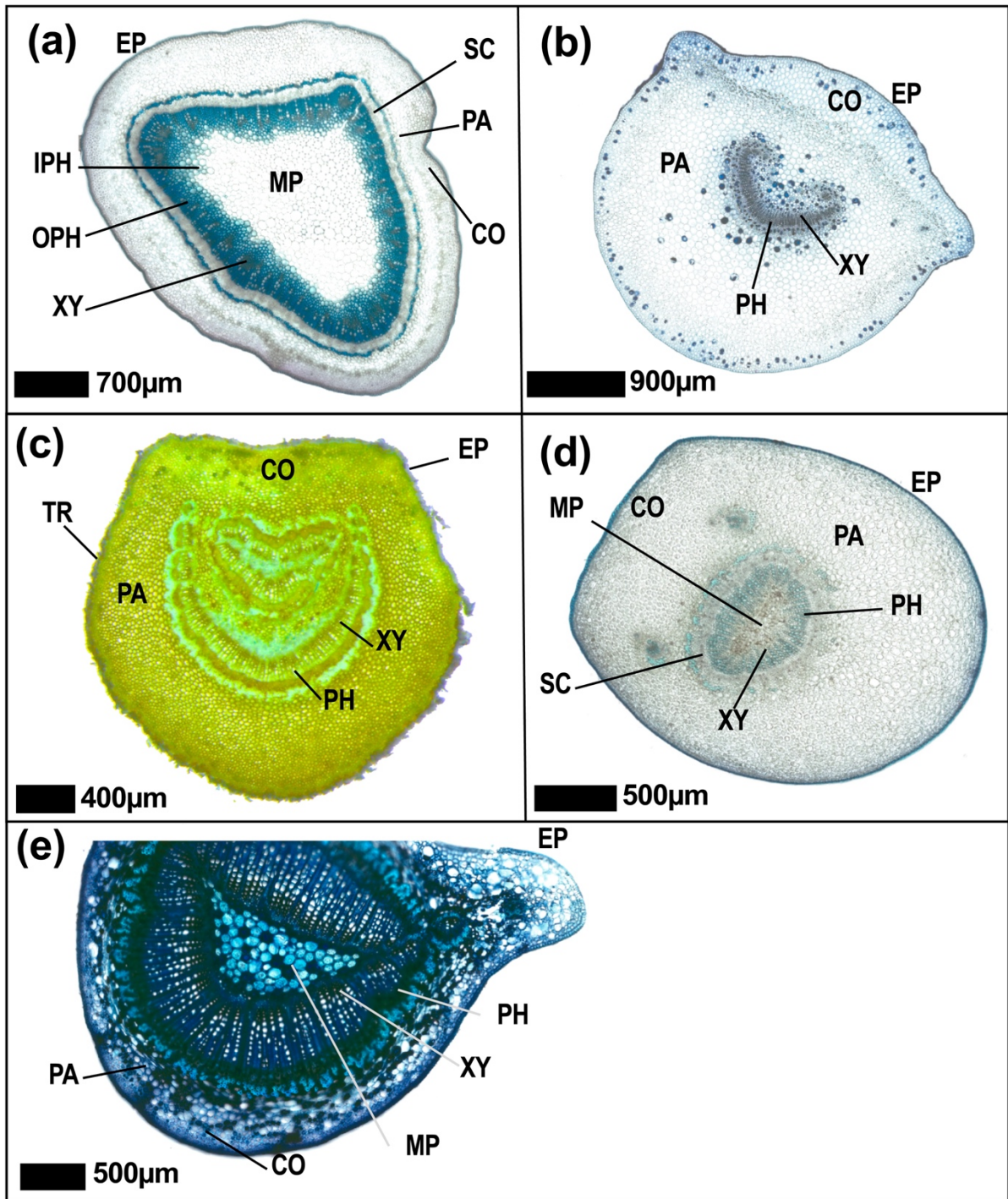
⁷Photon Science, Deutsches Elektronen-Synchrotron DESY, Germany.

* Corresponding author: a.vanderent@uq.edu.au

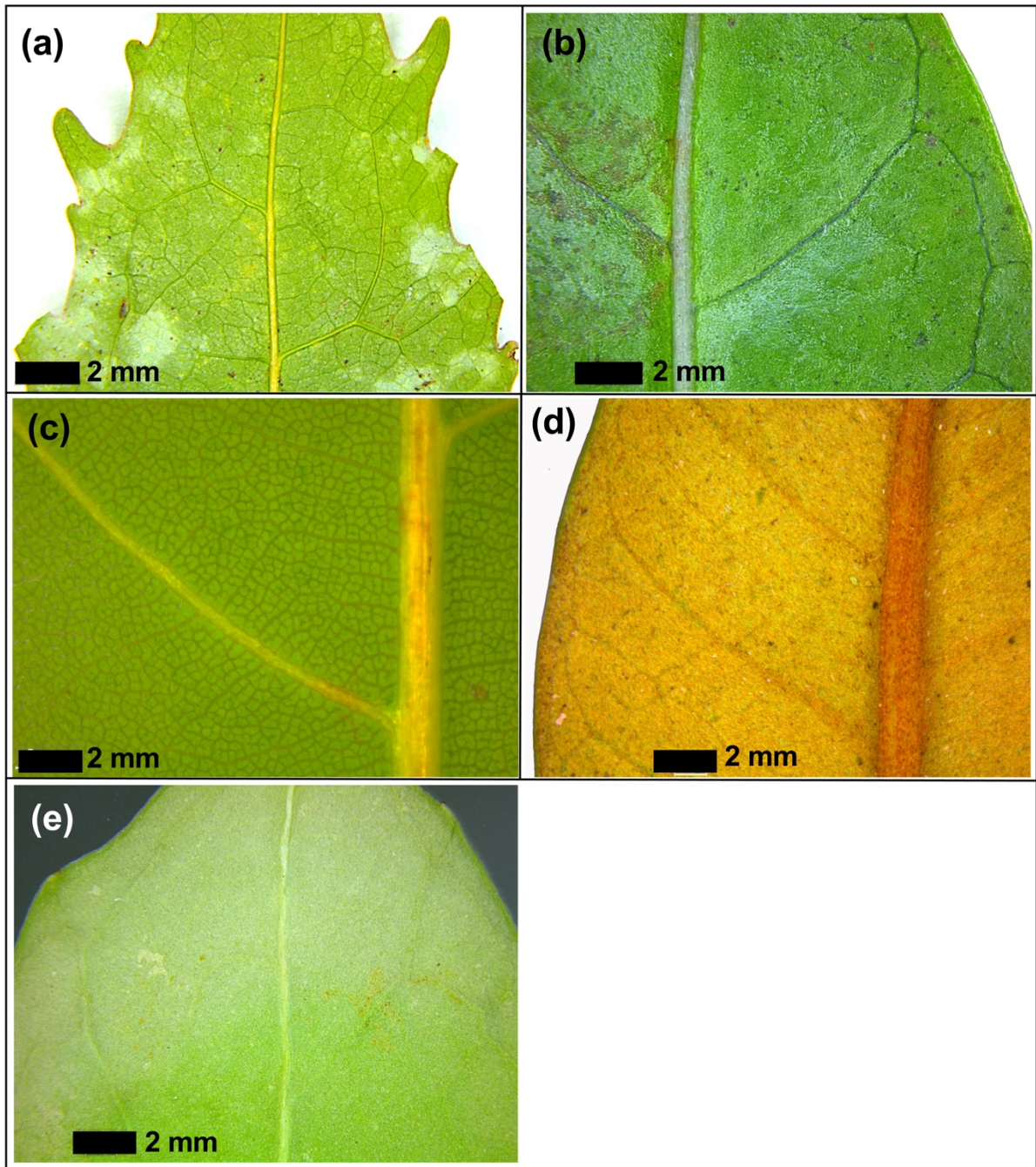
Phone: +61 (07) 3346 4003



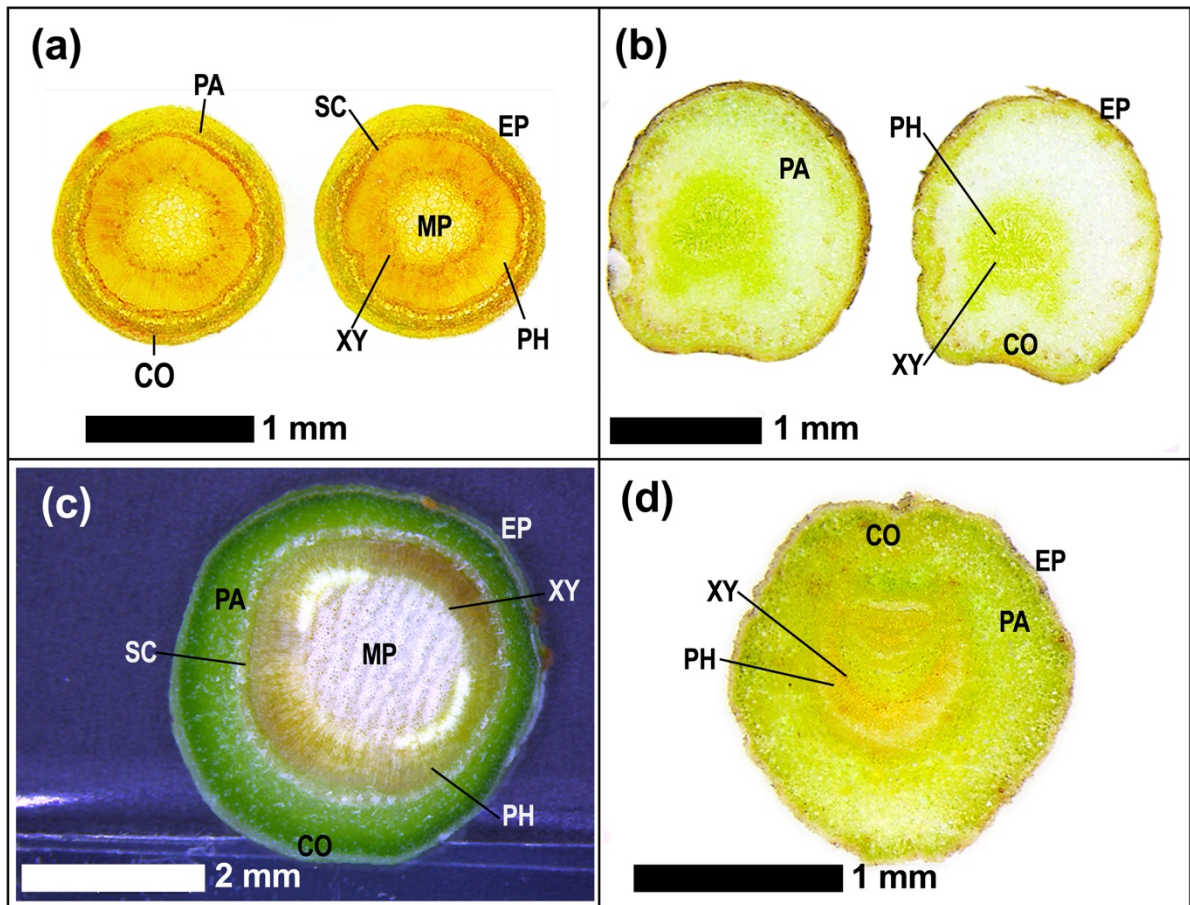
Suppl Fig 1. Light microscopy images of toluidine-stained cross-sections of midrib portions of *Hybanthus austrocaledonicus* (a), *Psychotria gabriellae* (b), *Pycnandra acuminata* (c), *Homalium francii* (d), and *Geissois pruinosa* var. *pruinosa* (e). Abbreviations annotated of anatomical features: *UE* upper epidermis, *LE* lower epidermis, *CO* collenchyma, *PM* palisade mesophyll, *SM* spongy mesophyll, *XY* xylem, *PH* phloem; *TR* trichomes



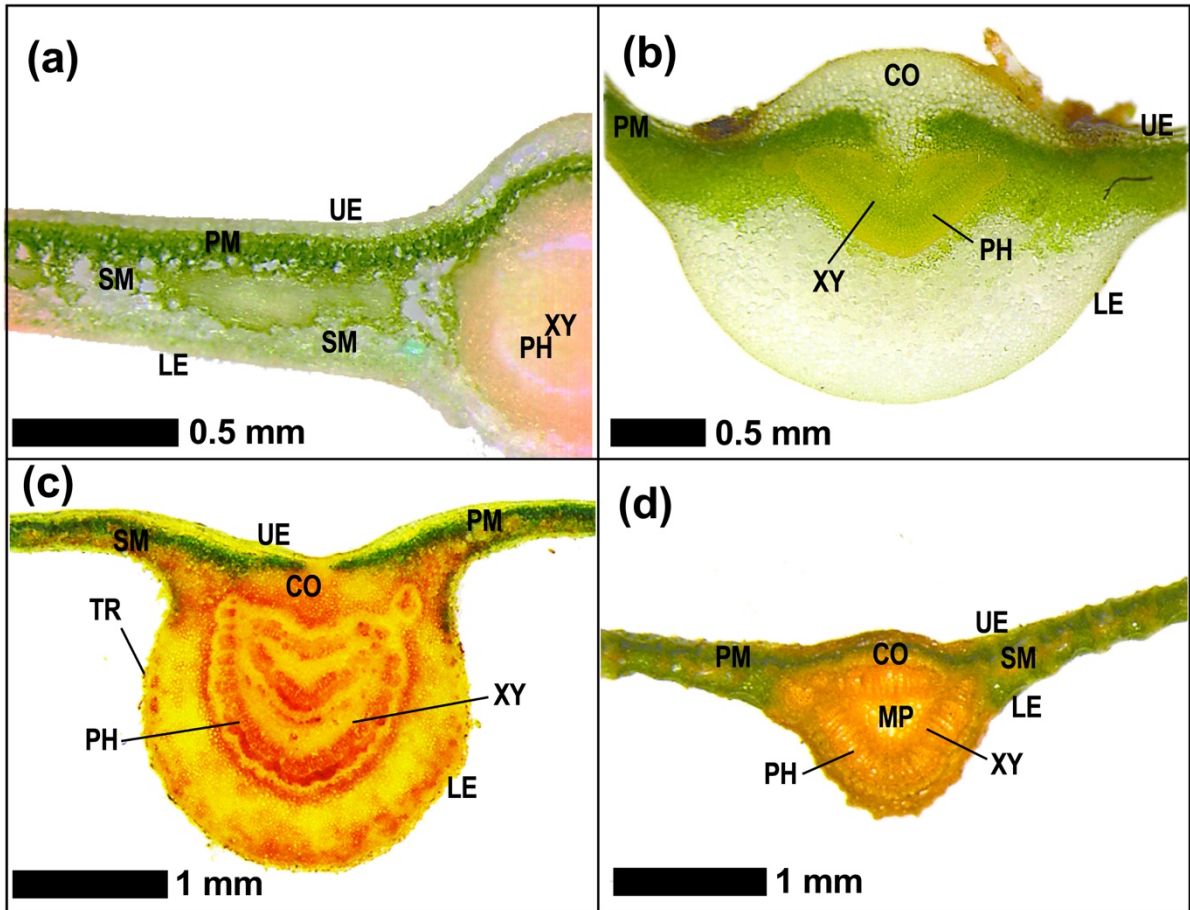
Suppl Fig 2. Light microscopy images of toluidine-stained cross-sections of petioles of *Hybanthus austrocaledonicus* (a), *Psychotria gabriellae* (b), *Pycnandra acuminata* (c), *Homalium francii* (d), and *Geissois pruinosa* var. *pruinosa* (e). Abbreviations annotated of anatomical features: *EP* epidermis, *CO* collenchyma, *PA* parenchyma, *SC* sclerenchyma, *MP* medullar parenchyma, *XY* xylem, *PH* phloem; *TR* trichomes



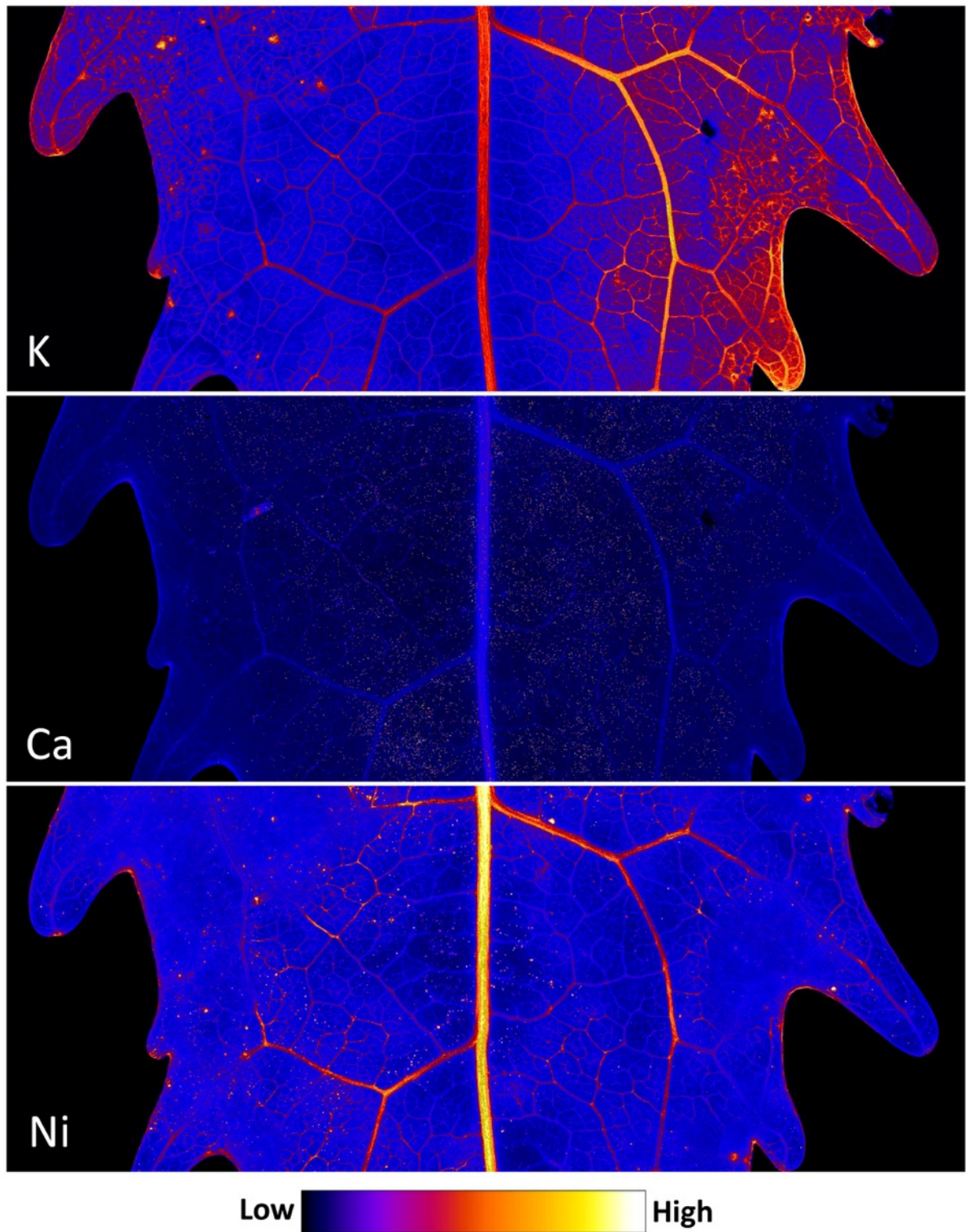
Suppl Fig 3. Light microscopy images of non-stained leaf portions of *Homalium francii* (a), *Psychotria gabriellae* (b), *Geissois pruinosa* var. *pruinosa* (c), *Pycnantra acuminata* (d), and *Hybanthus austrocaledonicus* (e) as analysed during the micro-X-ray Fluorescence (μ XRF) imaging.



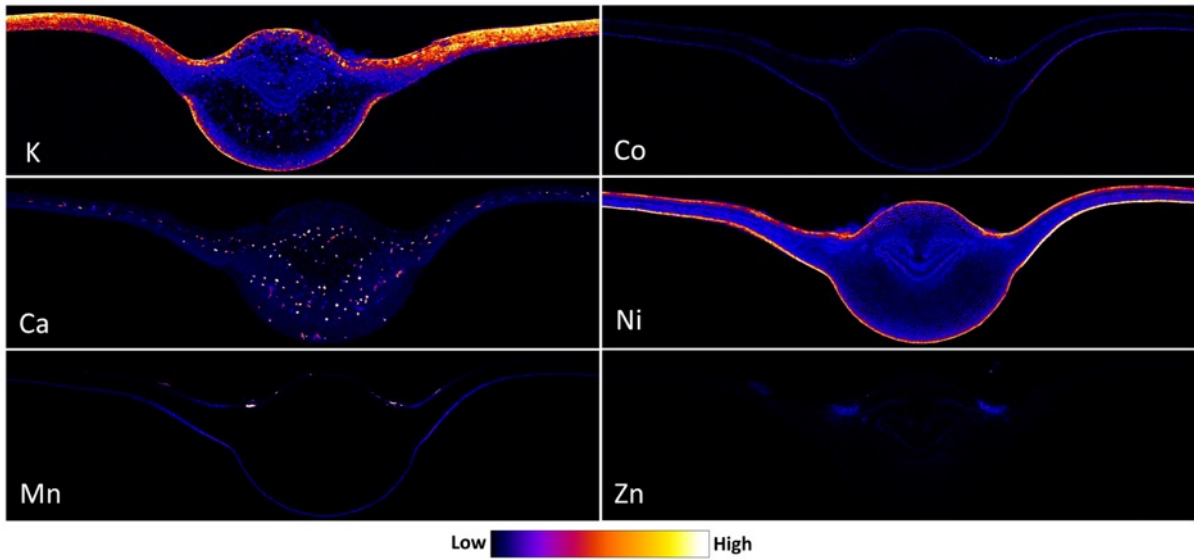
Suppl Fig 4. Light microscopy images of non-stained petiole cross-sections of *Geissois pruinosa* var. *pruinosa* (a), *Homalium francii* (b), *Hybanthus* (c), and *Pycnandra acuminata* (d) as analysed during the micro-X-ray Fluorescence (μ XRF) imaging. Abbreviations annotated of anatomical features: *EP* epidermis, *CO* collenchyma, *PA* parenchyma, *SC* sclerenchyma, *MP* medullar parenchyma, *PH* phloem, *XY* xylem



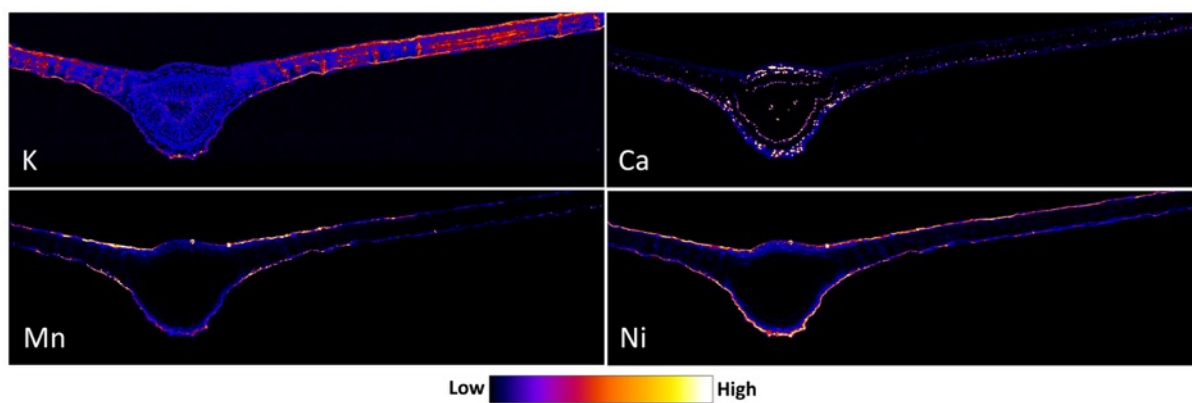
Suppl Fig 5. Light microscopy images of non-stained midrib cross-sections of *Hybanthus austrocaledonicus* (a), *Psychotria gabriellae* (b), *Pycnantha acuminata* (c), and *Geissois pruinosa* var. *pruinosa* (d) as analysed during the micro-X-ray Fluorescence (μ XRF) imaging. Abbreviations annotated of anatomical features: *UE* upper epidermis, *LE* lower epidermis, *CO* collenchyma, *PM* palisade mesophyll, *SM* spongy mesophyll, *XY* xylem, *PH* phloem, *MP* medullar parenchyma, *TR* trichomes



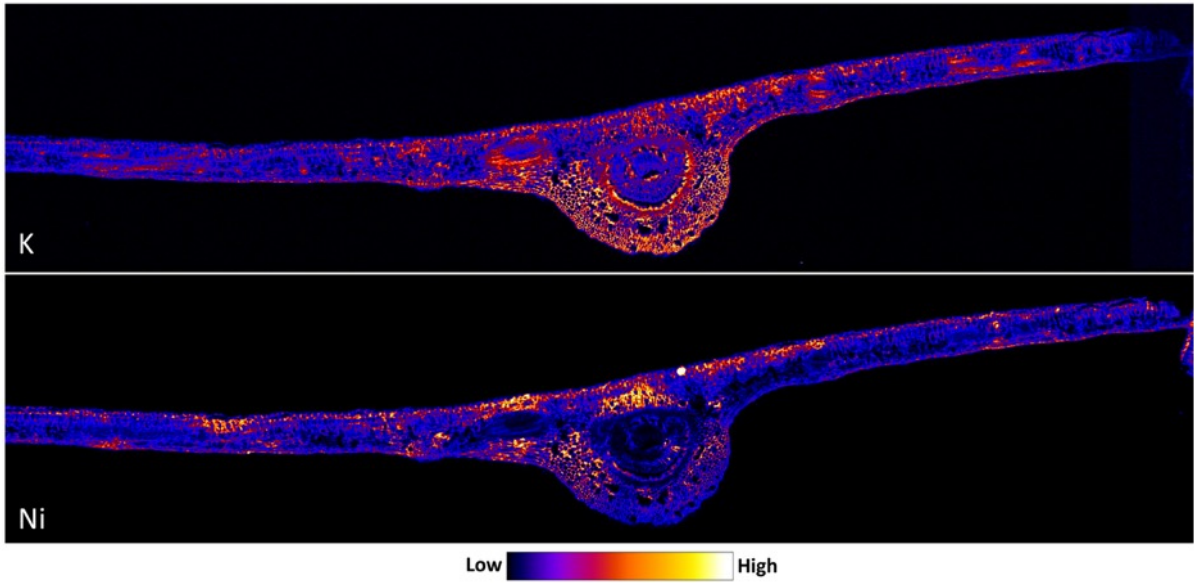
Suppl Fig 6. Synchrotron μ XRF maps of K, Ca, and Ni of a freeze-dried intact leaf portions of *Homalium francii*. The maps measure $18.57 \times 7.46 \text{ mm}^2$ at $10\mu\text{m}$ resolution with 12 ms dwell. Maps were cropped to fit figure panels.



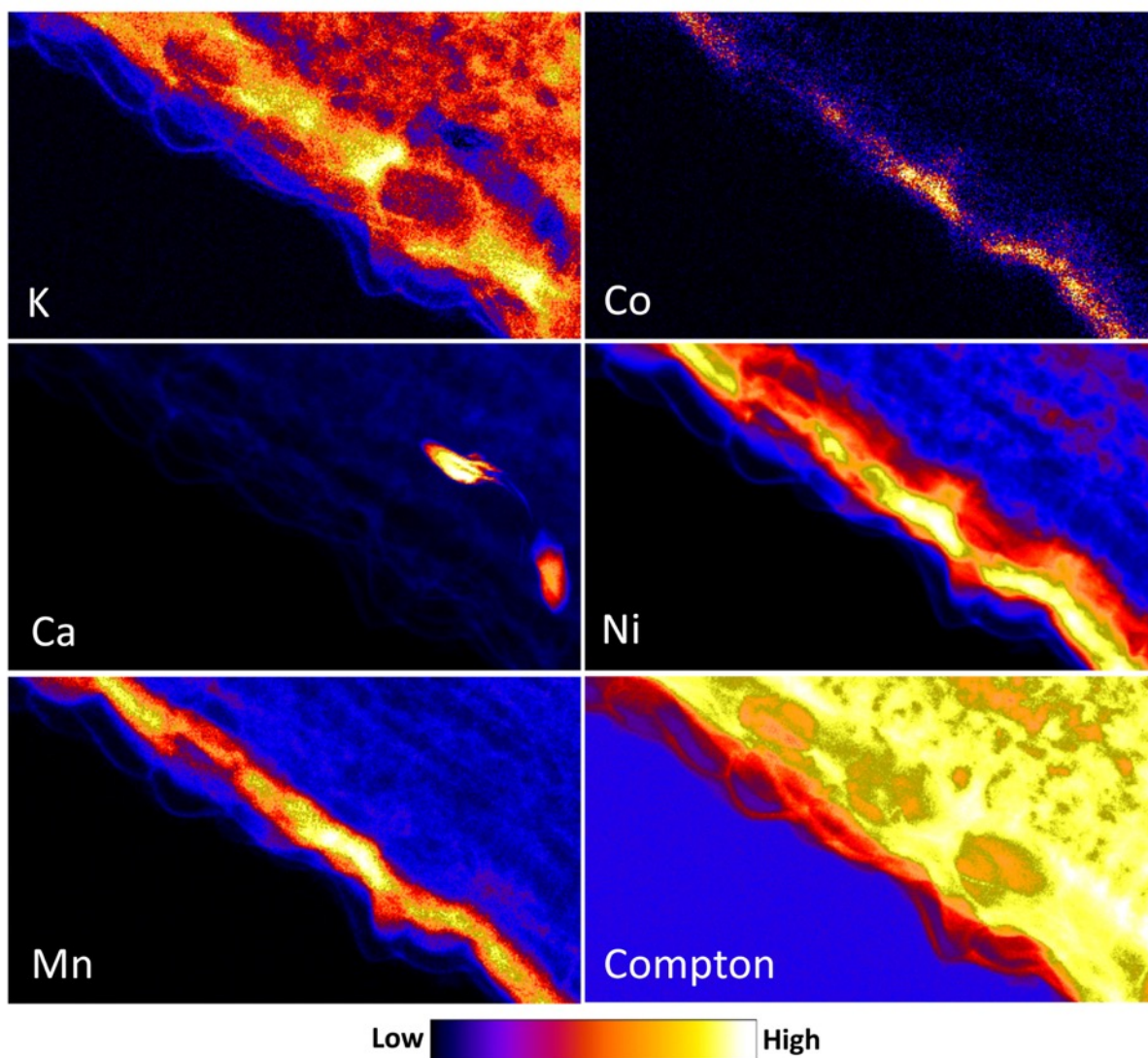
Suppl Fig 7. Synchrotron μ XRF maps of K, Co, Ca, Ni, Mn and Zn of a fresh leaf cross section portion of *Psychotria gabriellae*. The maps measure $8.52 \times 5.78 \text{ mm}^2$ at $8 \text{ }\mu\text{m}$ resolution with 10 ms dwell. Maps were cropped to fit figure panels.



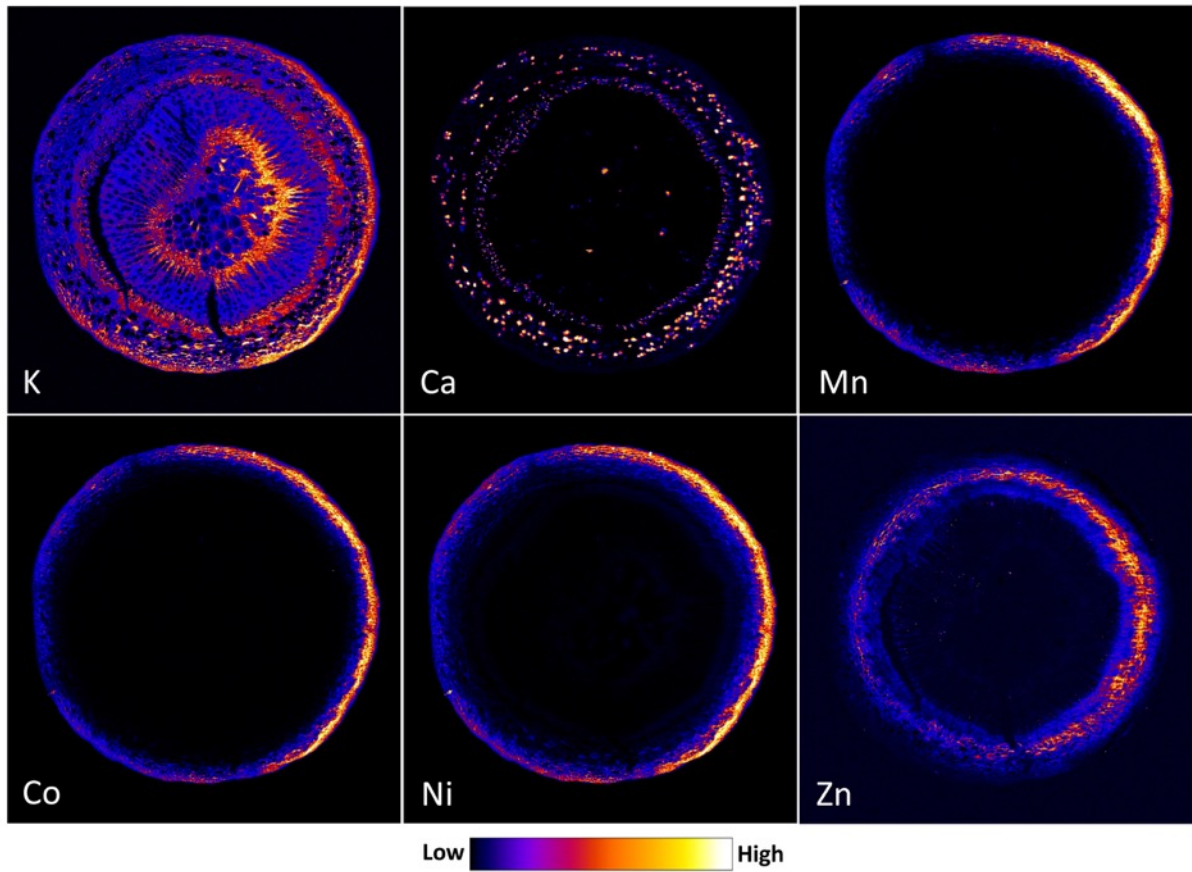
Suppl Fig 8. Synchrotron μ XRF maps of K, Ca, Ni and Mn of a fresh leaf cross section portion of *Geissois pruinosa* var. *pruinosa*. The maps measure $7.68 \times 2.25 \text{ mm}^2$ at $7 \mu\text{m}$ resolution with 10 ms dwell. Maps were cropped to fit figure panels.



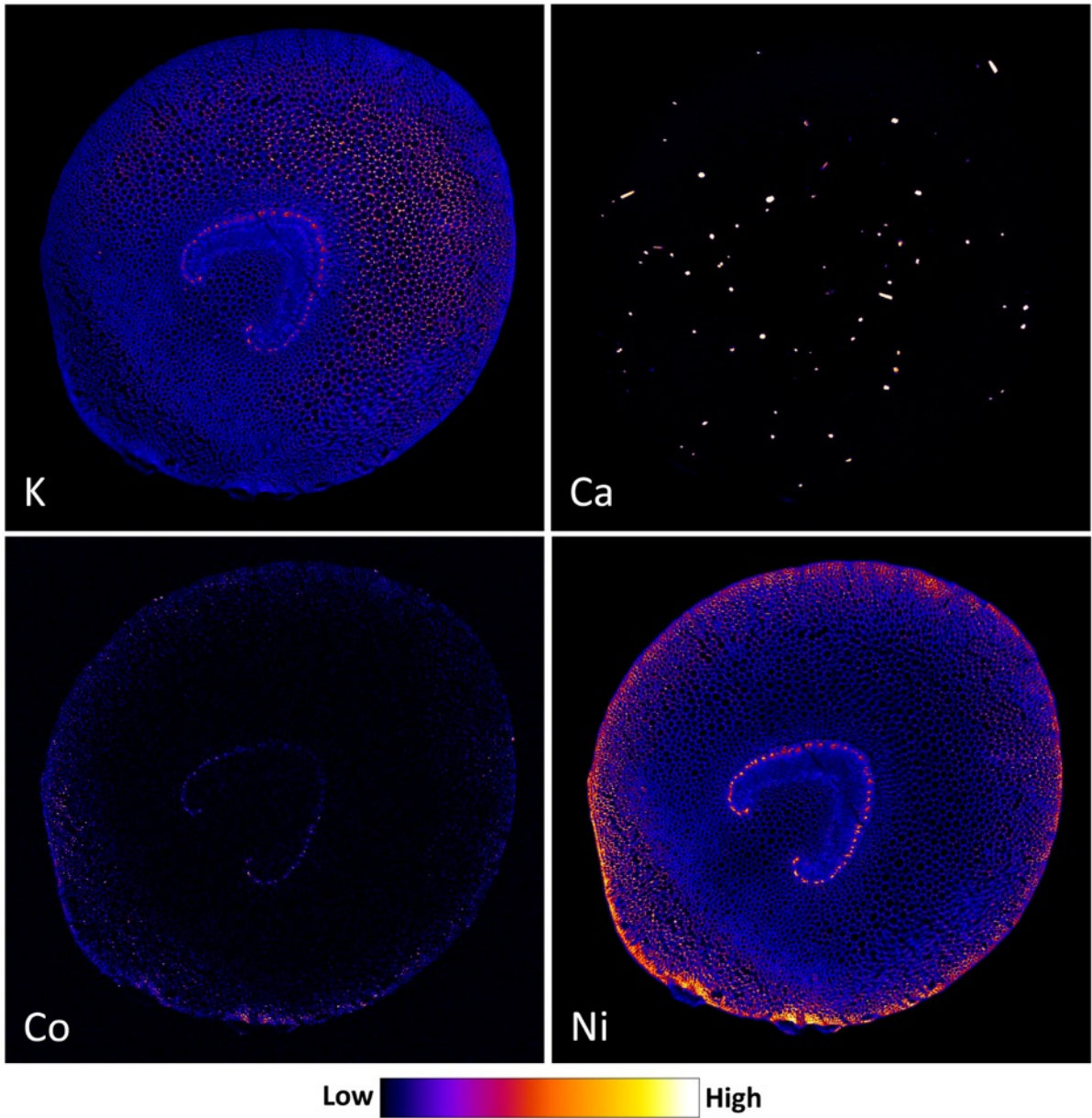
Suppl Fig 9. Synchrotron μ XRF maps of K, and Ni of a freeze-dried leaf cross section portion of *Hybanthus austrocaledonicus*. The maps measure $7.07 \times 1.60 \text{ mm}^2$ at $5 \text{ }\mu\text{m}$ resolution with 10 ms dwell. Maps were cropped to fit figure panels.



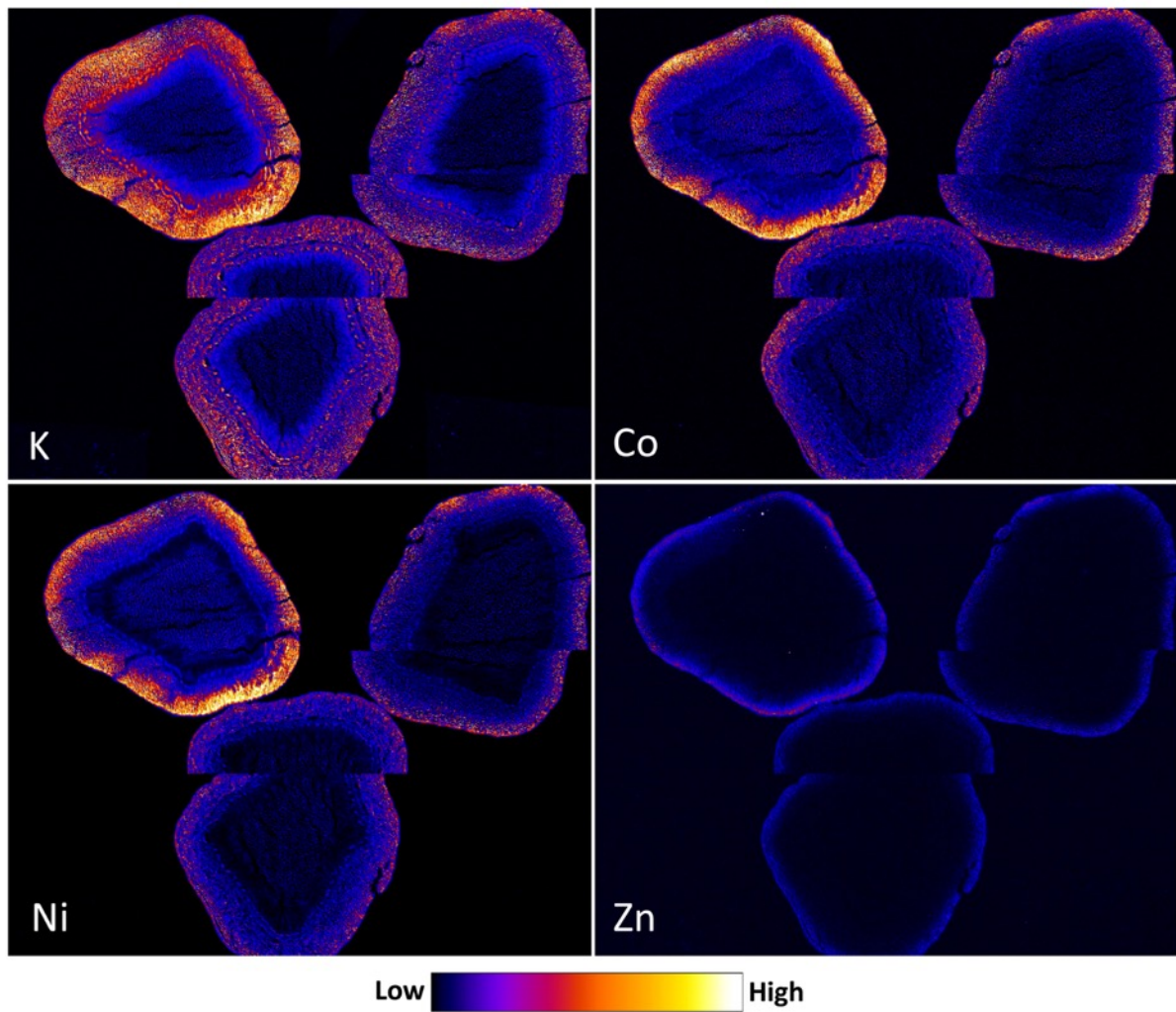
Suppl Fig 10. Synchrotron μ XRF maps of K, Co, Ca, Ni, Mn and Compton Scattering of a fresh leaf blade cross section portion of *Psychotria gabriellae*. The maps measure 0.30×0.17 mm² at 8 μ m resolution with 10 ms dwell. Maps were cropped to fit figure panels.



Suppl Fig 11. Synchrotron μ XRF maps of K, Co, Ca, Ni, Mn and Zn of a fresh leaf petiole cross-section portions of *Geissois pruinosa* var. *pruinosa*. The maps measure 2.90×3.01 mm² at 5 μ m resolution with 10 ms dwell. Maps were cropped to fit figure panels.



Suppl Fig 12. Synchrotron μ XRF maps of K, Co, Ca, and Ni of a freeze-dried petiole of *Psychotria gabriellae*. The maps measure $4.00 \times 3.91 \text{ mm}^2$ at $6 \mu\text{m}$ resolution with 10 ms dwell. Maps were cropped to fit figure panels.



Suppl Fig 13. Synchrotron μ XRF maps of K, Co, Ni and Zn of a freeze-dried twig cross section portions of *Hybanthus austrocaledonicus*. The maps measure $6.70 \times 5.41 \text{ mm}^2$ at $9 \mu\text{m}$ resolution with 10 ms dwell. Maps were cropped to fit figure panels.